applied sciences

MDPI

Article

Investigation of Debonding Effect in Internal Replacement Pipe System Under Lateral Loading

Tri C. M. Tien [1,*], Allan Manalo [1], Patrick Dixon [2], Warna Karunasena [1], Hamid Ahmadi [1], Shanika Kiriella [1], Ahmad Salah [1] and Brad P. Wham [2]

[1] Centre for Future Materials, University of Southern Queensland, Toowoomba, QLD 4350, Australia; allan.manalo@unisq.edu.au (A.M.); karu.karunasena@unisq.edu.au (W.K.); hamid.ahmadi@unisq.edu.au (H.A.); shanika.kiriella@unisq.edu.au (S.K.)

[2] Center for Infrastructure, Energy, and Space Testing, University of Colorado Boulder, Boulder, CO 80309, USA; padi9036@colorado.edu (P.D.)

* Correspondence: camminhtri.tien@unisq.edu.au

Featured Application: Rehabilitation of Oil and Gas Pipelines.

Abstract: The aging pipeline infrastructure around the world necessitates immediate rehabilitation. Internal replacement pipe (IRP) is a trenchless system offering a versatile and cost-effective solution across a variety of industries, including oil, natural gas, water, and wastewater. As a structural pipeline repair system, IRPs are subject to lateral deformation because of surface traffic loading. The present study evaluates the impact of adhesion between the host pipe and the IRP, with a focus on assessing the debonding effect on the behavior of the repair system under lateral deformation and bending. This was achieved using a comprehensive approach, including experimental, numerical, and analytical techniques. Varying levels of adhesive strength resulting from different methods of surface preparation were considered. The effectiveness of the IRP system on both discontinuous host pipes with various crack widths and continuous host pipes was also investigated. The results demonstrate that adhesive strength exerts a significant influence on the repair system, especially in the case of narrow circumferential cracks, while its impact on the continuous system is minimal. For optimal performance, it is essential to choose adhesives that possess sufficient shear strength while also accounting for the required debonding length. This approach ensures that minor discontinuities are effectively controlled, thereby enhancing the system's fatigue life. The reliable determination of the maximum allowable shear strength for the adhesive or the debonding length can ensure that it does not negatively affect fatigue life. The findings presented in this study offer new insights into the development of trenchless repair techniques that can enhance system performance and extend service life.

Keywords: internal replacement pipe; trenchless; discontinuous; adhesive; surface preparation; bonding; debonding; shear strength

Citation: Tien, T.C.M.; Manalo, A.; Dixon, P.; Karunasena, W.; Ahmadi, H.; Kiriella, S.; Salah, A.; Wham, B.P. Investigation of Debonding Effect in Internal Replacement Pipe System Under Lateral Loading. *Appl. Sci.* **2024**, *14*, 10509. https://doi.org/10.3390/app142210509

Received: 27 August 2024
Revised: 16 October 2024
Accepted: 30 October 2024
Published: 14 November 2024

1. Introduction

Water, wastewater, oil, and natural gas are examples of critical resources that are conveyed using pipelines, which typically serve as efficient and reliable transportation systems. As these systems age, maintenance, repair, and eventual replacement become necessary to ensure continued safety and reliability. For example, according to reports in [1–7], most oil and gas pipelines in the United States, Europe, and Australia are over 40 years old and need attention. Regular maintenance and monitoring of pipelines are essential for ensuring their continued integrity. There is an increasing interest in modernizing pipeline systems among various stakeholders, with numerous examples of notable advancements. Policymakers and utilities are responsible for delivering natural gas to customers; for

example, they widely acknowledge the imperative to expedite ongoing endeavors in replacing outdated infrastructure while also adopting innovative approaches to operations and maintenance [8,9]. The integrity of buried pipelines is susceptible to multiple failure modes, encompassing corrosion, mechanical damage, material defects, and geohazards such as landslides and earthquakes. Among these failure modes, mechanical damage emerges as a prominent concern attributable to excavation activities, construction defects, or external forces, such as traffic loading, heavy equipment, or third-party interference. In practice, buried pipelines frequently face substantial transverse loads originating from excavation equipment or surface traffic, potentially jeopardizing their structural integrity [10]. The failure of pipelines is an unfortunate event with far-reaching consequences, encompassing economic, environmental, and, in extreme cases, human casualties [11,12]. Thus, it is essential to comprehend the failure modes associated with deflection to develop effective strategies for regulation, inspection, maintenance, and repair.

The rehabilitation of legacy pipes presents a crucial challenge in the modernization of aging infrastructure. Internal replacement pipe (IRP) technology is emerging as a promising solution to address this problem. IRP is a trenchless technology that involves the installation of a new, structurally reinforced pipe within the existing pipeline, thereby providing enhanced strength and longevity [13]. There are several benefits to using the IRP as a repair system for legacy pipelines. First, it eliminates the need for complete pipeline replacement, minimizing the associated costs, disruptions, and environmental impact. Second, IRP offers significant advantages over alternative methods by providing improved structural integrity, corrosion resistance, and increased capacity. Finally, IRP technology can be tailored to accommodate varying pipe diameters and lengths, making it suitable for a wide range of legacy pipeline rehabilitation projects. Recent studies have demonstrated the effectiveness of IRP technology in rehabilitating legacy pipelines. For instance, Sirimanna et al. [14] showed that IRP can significantly enhance the structural integrity of deteriorated pipes. Research activities have demonstrated that the use of IRP increases the load-bearing capacity of pipes while concurrently reducing the probability of leaks or failures [15–19]. The report produced by the U.S. Department of Energy emphasized the environmental benefits of IRP in natural gas pipelines, highlighting its potential to reduce greenhouse gas emissions by reducing system integrity risks [8]. These findings highlight the importance of IRP as an innovative, cost-effective, and sustainable approach for rehabilitating legacy pipelines. This approach also ensures the safety and reliability of pipeline distribution systems while minimizing environmental impacts.

More precise estimates of the bending stiffness, nonlinearity, and debonding mechanism of composite sections are desired for the future development of the IRP trenchless technology [15–20]. In this study, the primary objective is to comprehensively investigate the behavior and response of IRP under lateral loads. To achieve this, a multifaceted approach combining experimental data analysis, numerical simulation, and analytical calculation is employed. On the one hand, these experimental data provide essential insights into the physical response of the IRP when subjected to lateral loads, allowing for an in-depth understanding of its structural behavior. On the other hand, numerical simulations have been developed to model and predict the intricate response of the IRP under different lateral load scenarios, offering a virtual platform for further analysis and optimization. To complement these experimental and numerical approaches, a standard analytical calculation is employed, enabling the formulation of mathematical expressions that capture the essential mechanical properties and responses of the four-point bending mechanism. By synergistically integrating these three methodologies, a comprehensive understanding of the complex behavior of IRP under lateral loads is achieved. This study focuses on numerical investigation of the impact of various surface preparation methods (unclean, cleaned, and ablated) on the adhesive strength of repair systems using a debonding finite element analysis (FEA) mechanism. This work includes a comprehensive parametric analysis of discontinuous host pipes with varying crack widths of 12.7 mm (0.5 inch) and 152.4 mm (6 inch), as well as continuous host pipes. It also highlights the

critical role of adhesive strength in the IRP repair method, which is essential for optimizing the design and application of trenchless repair systems. This optimization leads to more efficient, cost-effective, and durable infrastructure maintenance solutions. The findings from this research provide valuable insights for advancing trenchless repair techniques, with the potential to improve system performance and extend service life.

The sections of the paper are organized as follows: Section 2 details the FEA methodology, covering the modeling techniques and validation of results, with particular emphasis on debonding phenomena. Section 3 explores the influence of surface preparation on debonding behavior. Finally, Section 4 concludes the paper by summarising the key findings and discussing their implications for advancing IRP technology.

2. Finite Element Analysis

2.1. Four-Point Bending Deflection Modelling and Validation

2.1.1. Four-Point Bending Deflection Modelling

It is essential to account for the most severe conditions expected over a 50-year design lifespan when determining the imposed loading protocols for buried pipelines subjected to lateral loading or bending due to traffic. A worst-case scenario can be modeled by introducing a complete circumferential fracture or crack along the pipe specimens [17]. In this work, finite element analysis (FEA) simulations were conducted using ANSYS/Mechanical software 2023 R2 to investigate the behavior of pipelines under lateral loading. Three-dimensional (3D) finite element models were created to simulate the conditions specified in the experimental setup conducted at the University of Colorado Boulder, as detailed in [17]. The center-to-center dimensions of the four-point bending setup were maintained at 63.5 cm by 101.6 cm by 63.5 cm (25 inches by 40 inches by 25 inches), as shown in Figure 1. The deflection measurement was zeroed at the initial stage of the experiment before any lateral loading was applied.

A single cast iron pipe with an outer diameter of 342.9 mm (13.5 inches) and a wall thickness of 17.272 mm (0.68 inches) was utilized [15,17,18] to calibrate and validate the numerical results. The standard A48 Class 20 gray cast iron [21], with a modulus of elasticity (MOE) of 70 GPa (10,153 ksi) and a Poisson′s ratio of 0.29, is used. The chemical composition of the cast iron is listed in Table 1. The test system was subjected to a load of 157.3 kN (35.4 kip) to achieve a design displacement of approximately 1.78 mm (0.07 inches) at its midspan, corresponding to the nominal diameter and wall thickness of the pipe. The measured deflection represented the overhead traffic load experienced by a pavement and subgrade system directly above the pipeline [15–18]. The load was oriented parallel to the pipeline′s longitudinal axis [17,18]. By applying this load, the stresses and deformations experienced by the specimen represent worst-case scenarios under vibrational loading, aiming to achieve a design fatigue life of 1 million cycles, which corresponds to a 50-year service life as introduced by O'Rourke et al. in 1985 [18,19]. The 1 million cycles over a 50-year period equate to approximately 20,000 cycles per year. This fatigue life estimate was rounded up from the original value of 780,000 cycles based on the expected number of heavy truck crossings over 50 years.

Table 1. Chemical composition of ASTM A48 Class 20 gray cast iron [21].

Standard	C (%)	Si (%)	Mn (%)	P (%)	S (%)
ASTM A48 Class 20	3.2–3.5	1.8–2.4	0.5–0.9	0–0.12	0–0.12

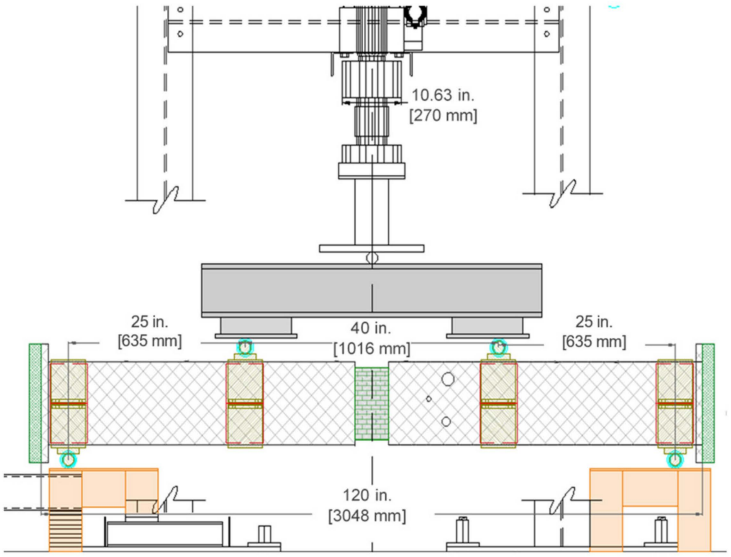

(**a**)

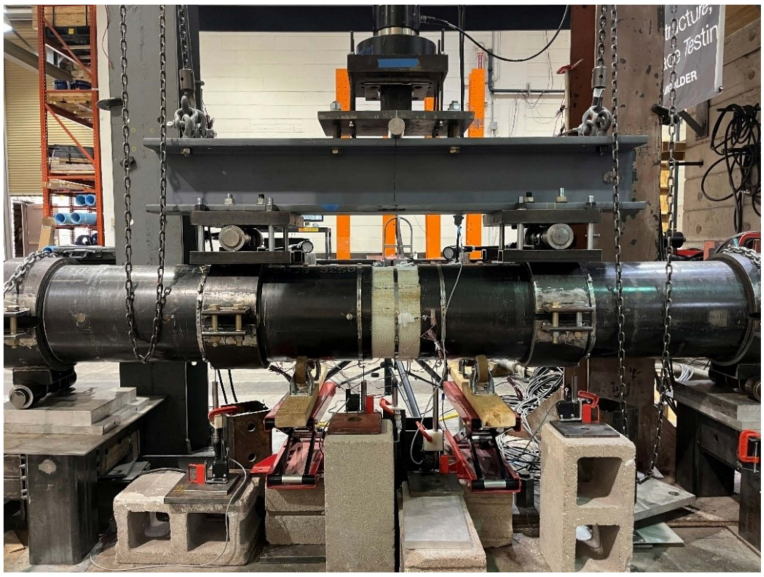

(**b**)

Figure 1. A demonstration of the deflection test pipe system: (**a**) schematic and (**b**) physical setup. Courtesy of images from the University of Colorado Boulder [17].

A linear static structural FEA was performed on a single cast iron pipe during a four-point bending assessment to validate the analytical approach using linear solution methods. Both ends of the pipe were capped with blind flanges, fully boned to the pipe. To ensure precise simulation of the mechanical contacts within the system, specifically the pin-lug and clamp-host pipe, a standard friction coefficient of 0.13 has been employed [20]. This selected value for the friction coefficient guarantees a realistic depiction of the frictional forces that arise during the interaction of these components. To simplify the model, a quarter of the system was simulated with symmetry boundary conditions applied in the longitudinal and transverse directions. A quarter FEA model and its components for the validation of single-pipe deflection are shown in Figure 2. An element size of 10 mm is used for the clamp, the loading head, and the blind. An optimal surface mesh size of 5×5 mm was chosen, as recommended in previous studies [18,19], to avoid redundant work in the pipe modeling. In the thickness direction, the number of elements was set to three, as illustrated in Figure 3. The model is composed of a total of 146,343 individual

elements. The standard ANSYS SOLID186 element [22] was used throughout the work, which incorporates capabilities such as plasticity, large deflection, and large strain.

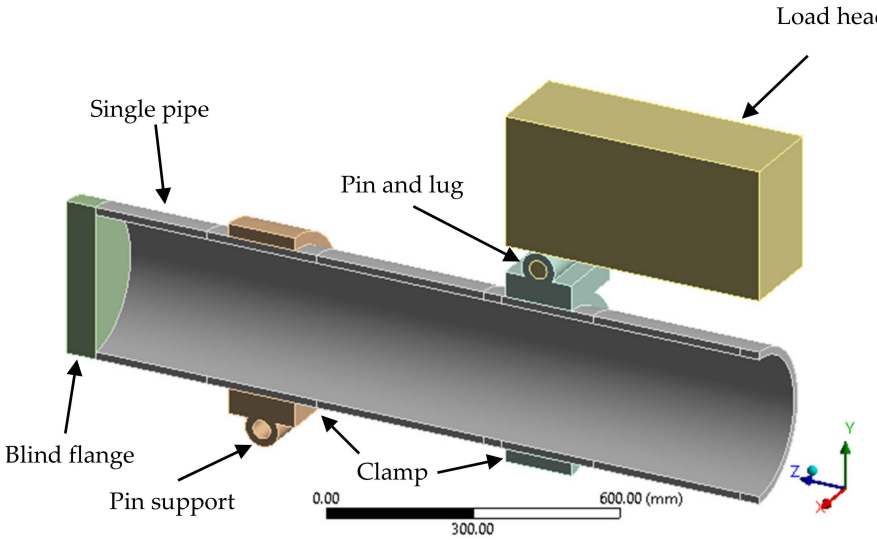

Figure 2. The four-point bending FEA modeling and its components for the single pipe deflection validation.

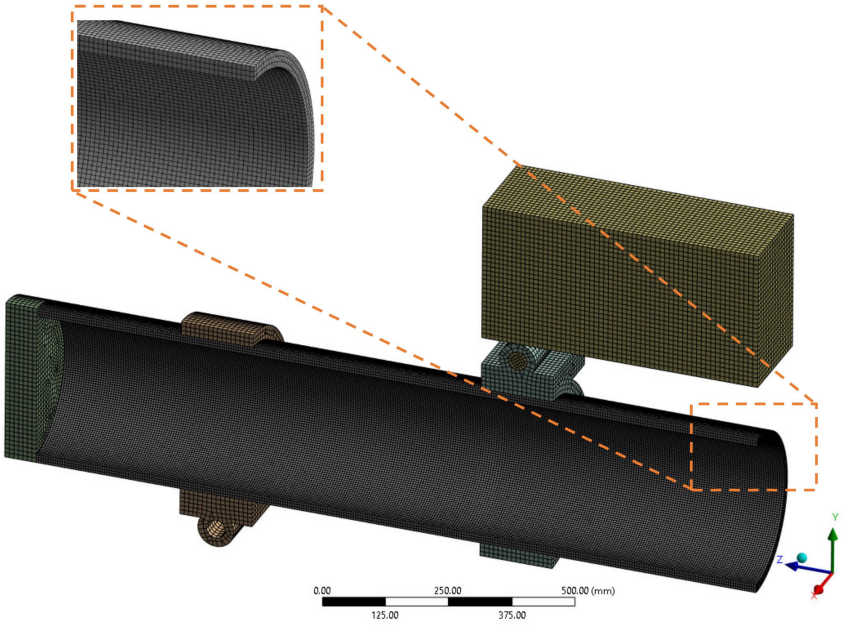

Figure 3. Meshing configurations for the single pipe deflection validation.

2.1.2. Four-Point Bending Deflection Validation

The accuracy and reliability of the four-point bending FEA model were validated by comparing the theoretically calculated values of tensile stress and midspan deflection of the single cast iron pipe. The elastic section modulus was utilized to evaluate the structural behavior of the circular hollow section. The elastic section modulus is a measure of a material's resistance to bending and is calculated using the following expression.

$$S = \frac{\pi\left(D_o^4 - D_i^4\right)}{32D_o}, \tag{1}$$

where D_o and D_i are the outer and inner diameters of the pipe, respectively.

The applied moment, denoted as M, is calculated using the following formula.

$$M = \frac{P}{2} x_L, \tag{2}$$

where P represents the applied load and x_L denotes the loading distance from the support, which is equal to 635 mm (25 inches) away.

The theoretical stress, denoted as σ, can be determined using the following formula.

$$\sigma = \frac{M}{S}, \tag{3}$$

where S is the cross-sectional modulus.

The tensile stresses and deflections at the bottom-most layer located at the midspan of the pipe, obtained through FEA models, exhibit a close correlation with the predicted tensile stresses determined through theoretical analysis, which are around 2% and 7% for the deflection and stress errors, respectively, as shown in Table 2. The consistency of the agreement is further supported by the coefficients of variation (COVs), which are found to be 5.529% and 0.772% for the deflection and stress errors, respectively.

Table 2. Validation of numerical and theoretical models for four-point bending deflection.

Load kN (kip)	Numerical Deflection mm (inch)	Analytical Deflection mm (inch)	Deflection Error %	Numerical Stress MPa (psi)	Analytical Stress MPa (psi)	Stress Error %
16 (4)	0.175 (0.00689)	0.178 (0.007)	1.742	3.375 (489.5)	3.645 (528.7)	7.413
31 (7)	0.350 (0.01380)	0.356 (0.014)	1.567	6.764 (981.1)	7.291 (1057.4)	7.224
47 (11)	0.526 (0.02069)	0.534 (0.021)	1.592	10.144 (1471.3)	10.936 (1586.1)	7.242
63 (14)	0.701 (0.02758)	0.712 (0.028)	1.614	13.522 (1961.3)	14.581 (2114.9)	7.263
79 (18)	0.875 (0.03447)	0.890 (0.035)	1.636	16.899 (2450.9)	18.227 (2643.6)	7.286
94 (21)	1.050 (0.04135)	1.068 (0.042)	1.657	20.276 (2940.8)	21.873 (3172.3)	7.301
110 (25)	1.225 (0.04822)	1.246 (0.049)	1.693	23.653 (3430.5)	25.517 (3701.0)	7.305
126 (28)	1.400 (0.05510)	1.424 (0.056)	1.721	27.029 (3920.2)	29.163 (4229.7)	7.317
142 (32)	1.573 (0.06194)	1.602 (0.063)	1.798	30.404 (4409.7)	32.808 (4758.5)	7.327
157 (35)	1.747 (0.06877)	1.780 (0.070)	1.860	33.769 (4897.7)	36.454 (5287.2)	7.365
COV (%)			5.529			0.772

2.2. Internal Replacement Pipe (IRP) System Modelling and Validation

2.2.1. IRP System Modelling

This section provides a detailed analysis of the nonlinear load-deformation characteristics of an IRP system. The system consists of a steel host pipe with a 12.7 mm (0.5 inch) wide circumferential discontinuity, which has been repaired using ALTRA10 supplied by Sanexen Environmental Service Incorporated. The analysis is conducted through a comprehensive investigation that includes 3D FEA simulations and experimental studies.

A 0.25 mm (0.01 inch) thick layer of epoxy adhesive is utilized to bond the host pipe and the IRP. In the FEA modeling, the contact conditions between the adhesive and the host pipe, as well as between the adhesive and the IRP, were assumed to be fully bonded. The pipe cavity is assumed to be filled with water, and a point mass representing the water is attached to the internal surface of the IRP and blind flange to simulate the experimental work. The water density is specified as 1000 kg/m^3. A total force of 71.2 kN (16 kip) is applied in the vertical direction to the loading head of the model to simulate the traffic load [17]. Additionally, an internal pressure of 0.448 MPa (65 psi) is applied on the inertial surfaces of the system to represent the operating pressure of a gas pipeline [17]. The standard earth gravity of 9.81 m/s^2 is considered, acting vertically on the entire model.

A nonlinear static structural FEA was conducted to capture large deformations and material plasticity in the study of the ALTRA10 internal replacement pipe (IRP) system,

where the IRP exhibits nonlinear stress-strain behavior. This nonlinear approach captures the effects of significant deformations and material-yielding factors that are essential for accurately understanding the true performance and potential failure modes of the structure, which linear assumptions would not adequately address. The FEA model is developed using the same parameters as the CUB test setup, which was discussed in the preceding section. The positions of interest for validation are 43.345 mm (1.7065 inches) and 591.833 mm (23.3005 inches) from the midspan of the system. Figure 4 depicts the FEA setup for the IRP system, illustrating the 12.7 mm (0.5 inch) discontinuity in the middle of the host pipe. This situation represents a full circumferential line crack in the IRP system. Furthermore, Tables 3 and 4 present the dimensions and material properties of the components used in the analysis. The mechanical properties of the steel components and epoxy adhesive were modeled as linear materials. Figure 5 shows the stress-strain nonlinear behavior of the ALTRA10 [23].

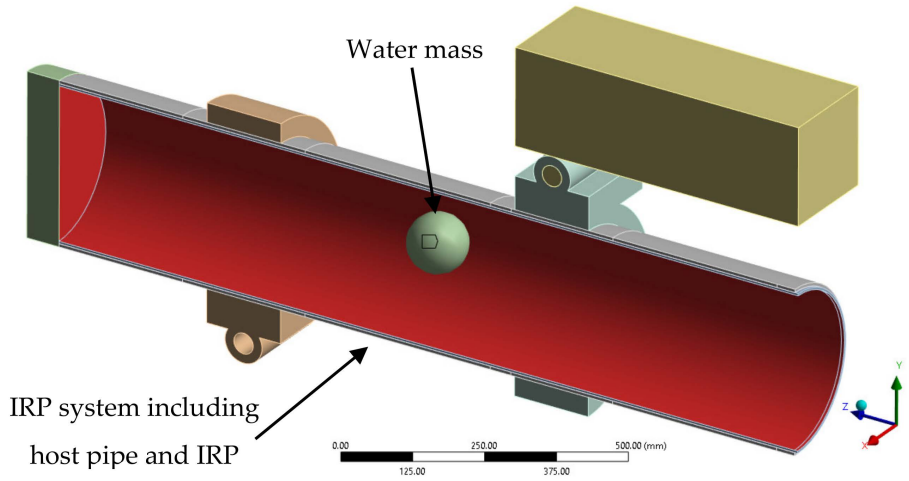

(**a**)

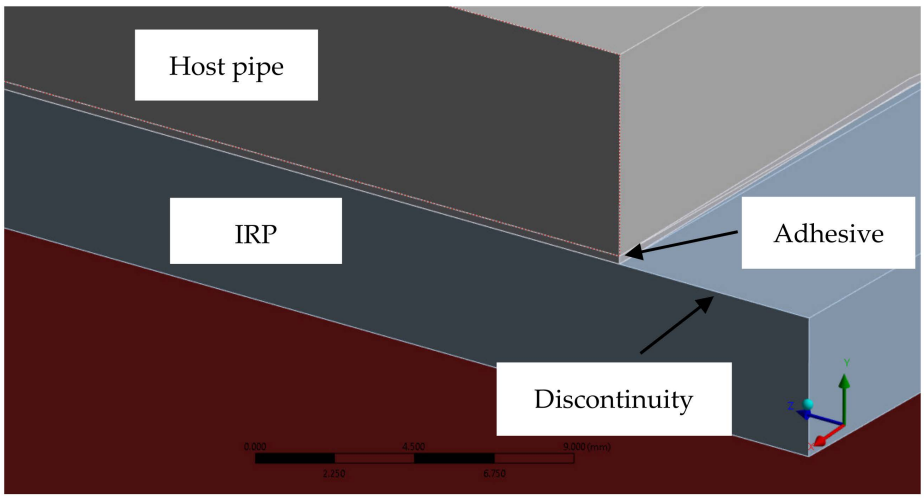

(**b**)

Figure 4. The modeling of the IRP system: (**a**) whole view and (**b**) discontinuity view.

Table 3. Dimensions of host pipe and IRP.

Host Pipe	IRP
Outer diameter: 323.85 mm (12.75 inches) Thickness: 6.35 mm (0.25 inches)	Outer diameter: 310.65 mm (12.23 in) Thickness: 4.115 mm (0.162 in)

Table 4. Properties of materials employed in the IRP system.

Properties	A36 Steel	ALTRA10 IRP	Epoxy Adhesive
Density kg/m^3 (lb/inch^3)	7850 (0.2836)	1000 (0.036127)	1150 (0.041546)
Elastic Modulus GPa (ksi)	200 (29,008)	3.74 (542)	2.59 (375)
Poisson's ratio	0.29	0.23	0.463

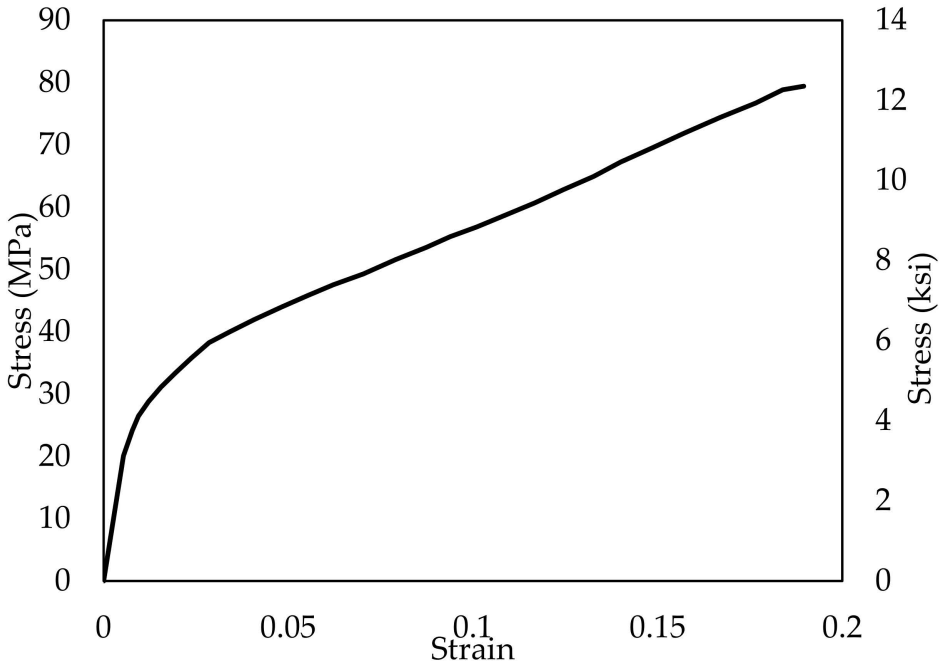

Figure 5. Stress and strain curve for ALTRA10 IRP.

2.2.2. IRP System Meshing

Figure 6 illustrates system meshing, an essential step in numerical simulations. Various components of the system, such as the clamp, pin, load head, and blind, have been assigned an element size of 10 mm (0.4 inch) [18]. This size provides a balance between computational efficiency and capturing the essential features of these components. An element size of 5 mm (0.2 inches) has been selected for the host pipe, IRP, and adhesive. Furthermore, an element size of 2 mm (0.08 inch) has been utilized for the crack opening region in the IRP. A bias factor of 5.0 and 2.0 is applied to the IRP and the discontinuity, respectively, with the finer end positioned toward the midspan. This smaller element size ensures a higher level of detail and accuracy in capturing the stress-intensity behavior and response of these critical elements within the system.

Regarding element thickness, three different thicknesses have been employed for the host pipe and IRP, enabling an appropriate representation of their structural integrity. Given the extremely thin aspect ratio of the adhesive, a single-element thickness has been chosen. As a result of the meticulous meshing process, a total of 181,003 elements have been recorded for the model. The comprehensive meshing scheme employed in this study aims to provide an accurate and detailed representation of the system's behavior and response under various loading conditions.

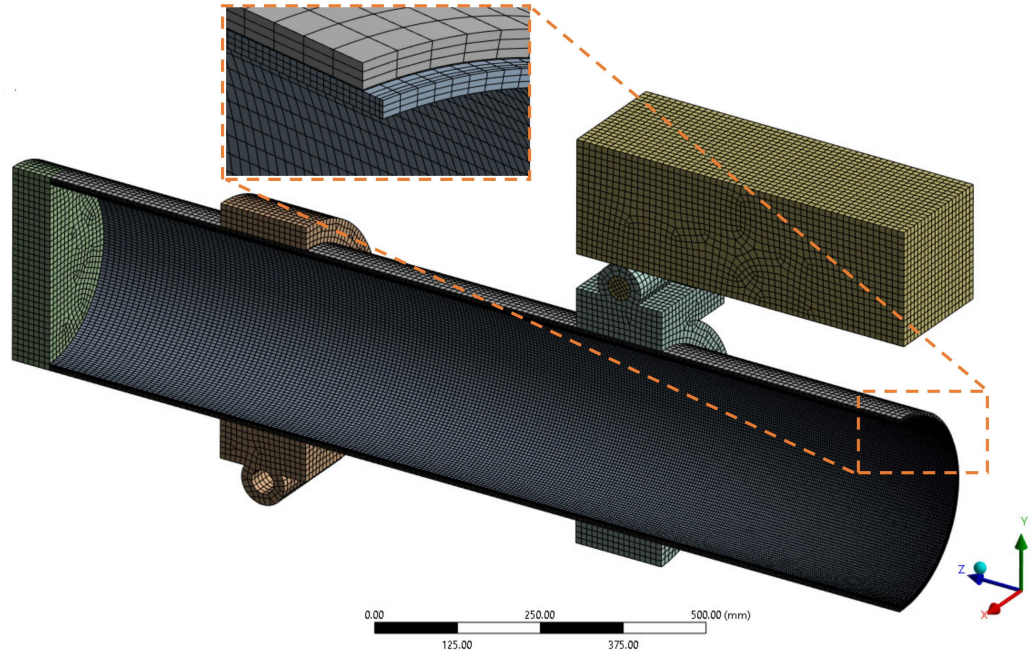

Figure 6. Meshing configurations for IRP system deflection.

2.2.3. IRP System Validation

A nonlinear static structural FEA approach is utilized to effectively depict and simulate the material nonlinearity exhibited by the IRP. To achieve this objective, the full Newton-Raphson solution procedure, a widely recognized iterative method for addressing nonlinear problems, is employed [18,19]. The FEA model accommodates substantial deformations and plasticity, ensuring a realistic representation of the IRP system's behavior under varying load conditions.

Figure 7 and Table 5 are a comparative analysis of load and displacement across various locations of the IRP system using FEA and experimental techniques. The findings demonstrate a favorable agreement up to a low load level of 21.4 kN (4.8 kip). At this point, a difference of 8% and 15% between the FEA and experimental results was observed for locations situated 43.3451 mm (1.7065 inches) and 591.8327 mm (23.3005 inches) away from the midspan, respectively. However, as the load magnitude increases, the disparity between the two methods amplifies. At the maximum load of 69.1 kN (15.5 kip), the difference increases to 20% and 26% at the respective locations mentioned earlier. In Figures 8 and 9, it is evident that at the maximum load of 69.1 kN (15.5 kip), a higher level of shear stress is observed within the adhesive layer situated between the host pipe and the IRP when compared with the pull-off stress, i.e., 28.75 MPa (4.17 ksi) versus 15.08 MPa (2.19 ksi), respectively. The shear stress is particularly prominent in the region adjacent to the discontinuity edge when compared with the pull-off stress. An analysis of Figure 7 reveals a distinct pattern in the unloading curve of the experimental sample, possibly indicating the occurrence of debonding in the adhesive layer between the host pipe and the IRP. This is evident from the noticeable decrease in strength during the unloading phase, suggesting the presence of structural weakening. The divergence in FEA and experimental results at higher levels of load is attributable to the debonding phenomenon occurring in the adhesive layer.

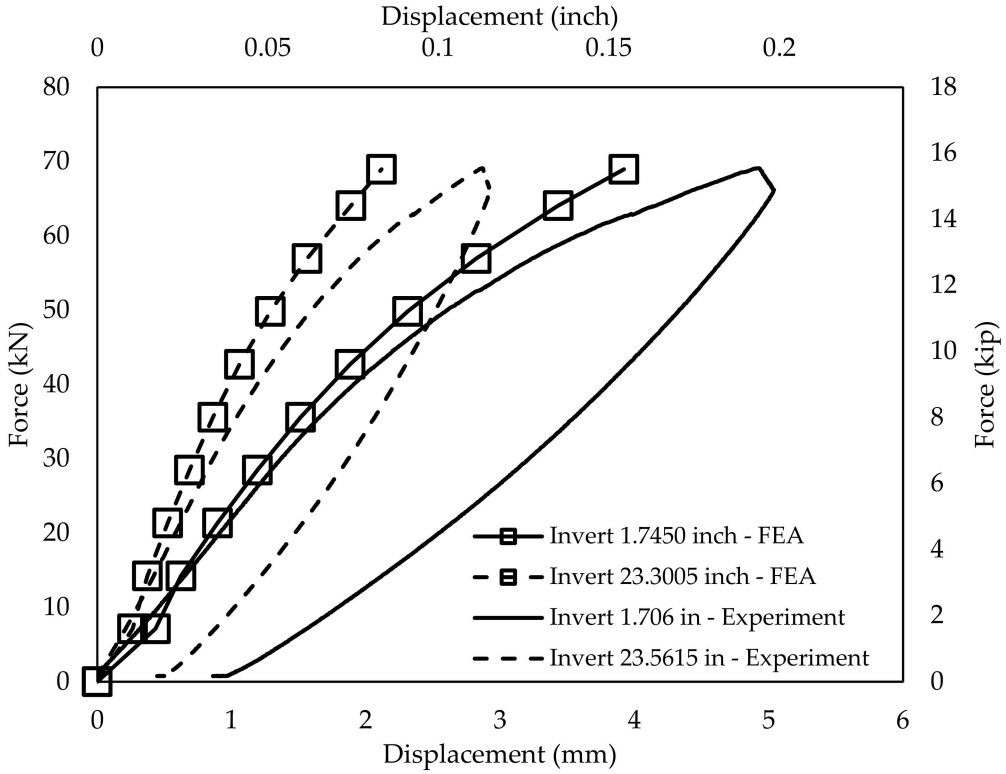

Figure 7. Validation of load-displacement relationship in the 12.7 mm (0.5 inch) discontinuous IRP system.

Table 5. Comparison of FEA and experimental results for the 12.7 mm (0.5 inch) discontinuous IRP system.

Load kN (kip)	Locations inch	Deflection, mm (inch)		Difference (%)
		FEA	Experiment	
21.4 (4.8)	1.7065	0.897 (0.035)	0.975 (0.038)	8
	23.3005	0.526 (0.021)	0.617 (0.024)	15
69.1 (15.5)	1.7065	3.922 (0.154)	4.925 (0.194)	20
	23.3005	2.116 (0.083)	2.855 (0.112)	26

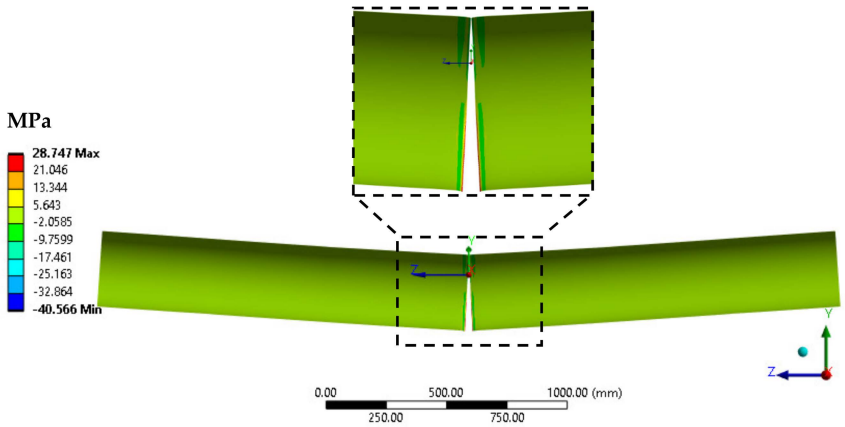

Figure 8. Shear stress results on the adhesive layer of the 12.7 mm (0.5 inch) discontinuous IRP system at a maximum load of 69.1 kN (15.5 kip) (magnified 18 times).

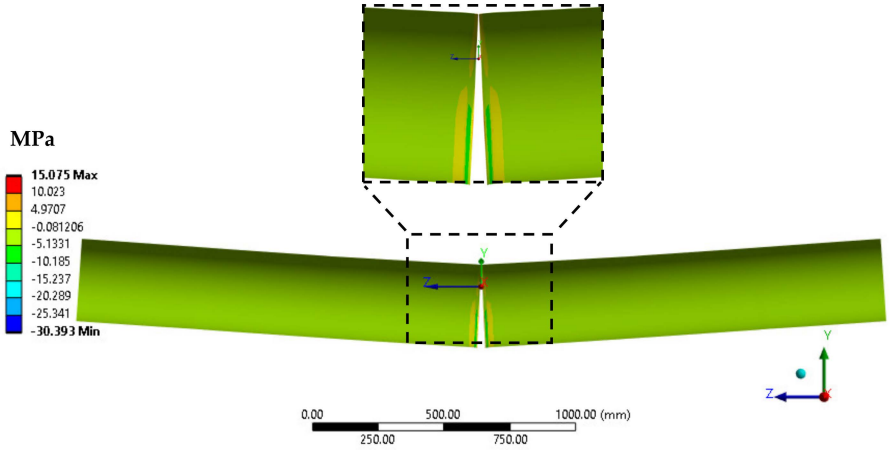

Figure 9. Pull-off stress results on the adhesive layer of the 12.7 mm (0.5 inch) discontinuous IRP system at a maximum load of 69.1 kN (15.5 kip) (magnified 18 times).

Figure 10 displays the equivalent stress on the IRP within the 12.7 mm (0.5 inch) discontinuous IRP system under the maximum load of 69.1 kN (15.5 kip). It can be observed that the highest equivalent stress, reaching 29.2 MPa (4.2 ksi), occurs at the bottom section of the IRP's discontinuity opening. Notably, this value remains below the strength of ALTRA10, which is 79.4 MPa (11.5 ksi). Consequently, it can be inferred that the IRP has not experienced failure up to the maximum load of 69.1 kN (15.5 kip).

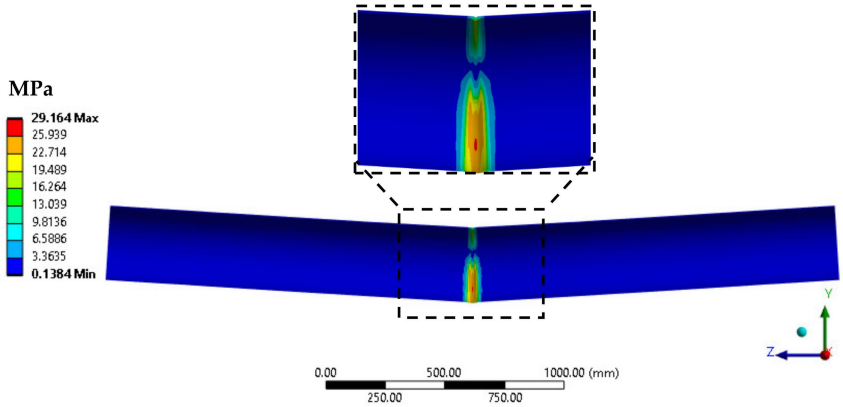

Figure 10. Equivalent stress results on the IRP of the 12.7 mm (0.5 inch) discontinuous IRP system at the system at 69.1 kN (15.5 kip) (magnified 25 times).

A series of tests were performed on a generic epoxy material. Those results showed that the epoxy had a pull-off strength of 19.58 MPa (2.84 ksi) and a shear strength of 4.95 MPa (0.72 ksi), resulting in an approximate ratio of 4:1. This significant disparity between pull-off and shear strengths indicates that shear stress is the predominant factor contributing to the failure of the adhesive layer. Accordingly, the following section provides a detailed analysis of the debonding mechanism in relation to the adhesive layer, with a particular focus on shear strength failure. The results from the generic epoxy testing were incorporated into the FEA model to achieve a more accurate numerical estimation of the experimental findings, thereby improving the precision of the overall analysis.

2.3. Debonding Mechanism Using Lap Shear Strength

2.3.1. Debonding Modelling and Validation

This section presents and validates the FEA modeling technique for the adhesive layer using lap shear strength as the primary metric. The numerical results are compared and verified against experimental data obtained from a flat cast iron sample. The adhesive

used in this study is a generic epoxy, which demonstrates a lap shear strength of 4.95 MPa (0.72 ksi) until adhesive failure occurs.

Figure 11 illustrates the geometry, constraints, and loading conditions employed in the FEA modeling, which adhere to the ASTM D5868 standard test method for lap shear adhesion in fiber-reinforced plastic (FRP) bonding [24]. The cast iron (CI) flat sample is fixed completely along a 50.8 mm (2 inch) section from the edge. The adhesive is placed between the CI flat sample and the IRP flat sample (presumably referring to the fiber-reinforced plastic). In the FEA model, the contact conditions between the adhesive and the flat samples were assumed to be fully bonded. The IRP sample is assumed to have the same Young's modulus of 2.59 GPa (375.07 ksi) and a Poisson's ratio of 0.463 as the adhesive. A force of 4.5 kN (1000 lbf) is applied longitudinally and outwardly along a 50.8 mm (2 inch) section from the edge of the IRP flat sample.

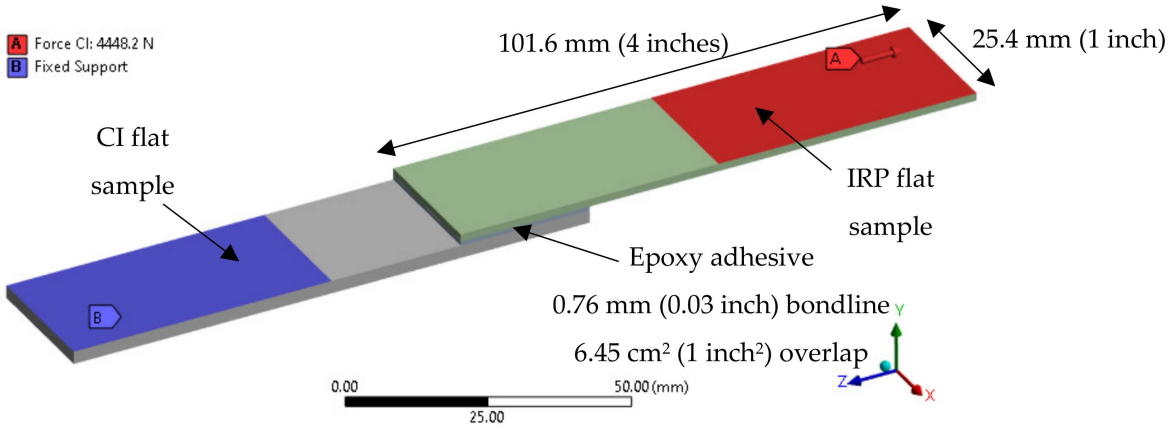

Figure 11. FEA modeling and constraints for the lap-shear test in accordance with ASTM D5868.

For the analysis, surface elements with dimensions of 2 mm × 2 mm (0.08 inch × 0.08 inch) were used, with three elements employed in the thickness direction, as depicted in Figure 12. A total of 4563 elements are employed and recorded using the standard ANSYS SOLID 186 elements.

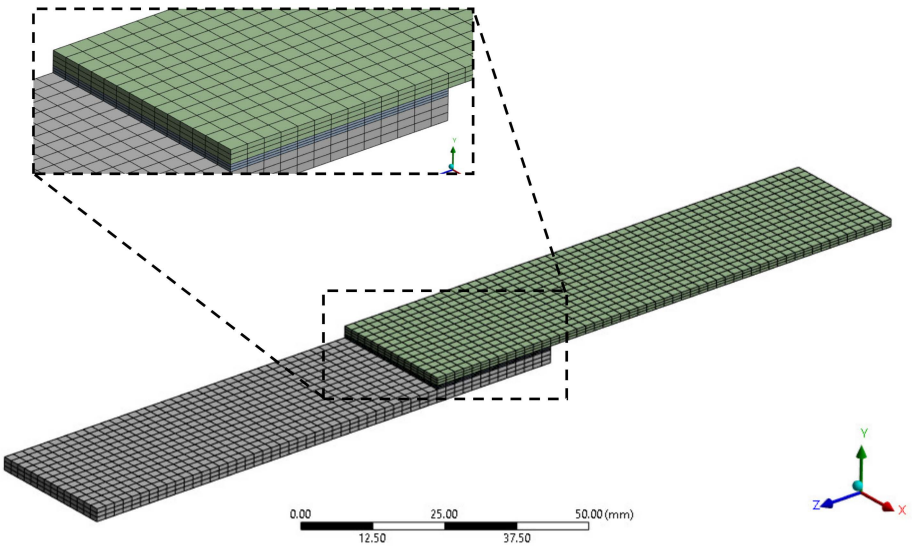

Figure 12. Meshing configuration of the lap-shear testing.

Based on the experimental results, the adhesive layer tends to fail when the applied load exceeds approximately 2.2 kN (500 lbf). This finding indicates that the shear stress in the adhesive layer surpasses 4.95 MPa (0.72 ksi) once the load exceeds 2.2 kN (500 lbf).

As shown in Figures 13 and 14, the adhesive material experiences a complete loss of strength, with most of the adhesive elements being removed due to excessive shear stress immediately after being subjected to a force of 2.2 kN (500 lbf). The numerical results align closely with the experimental findings, providing strong validation for using the lap-shear strength criterion for debonding in the numerical simulation of the IRP system.

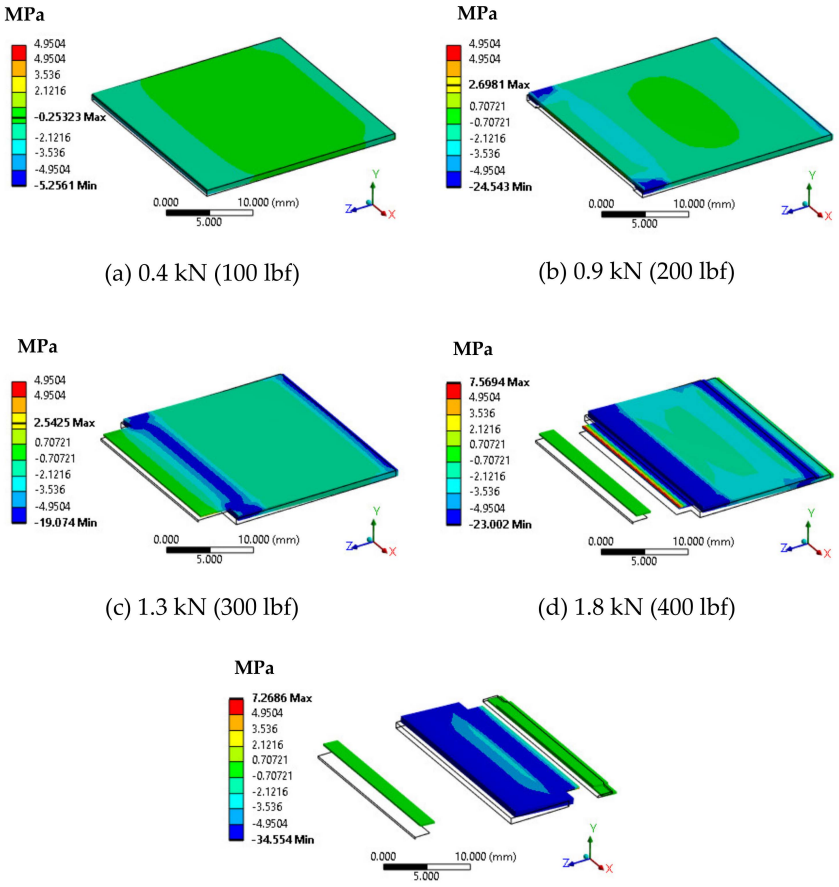

(a) 0.4 kN (100 lbf)

(b) 0.9 kN (200 lbf)

(c) 1.3 kN (300 lbf)

(d) 1.8 kN (400 lbf)

(e) 2.2 kN (500 lbf)

Figure 13. The debonding progression of the adhesive layer with load increment.

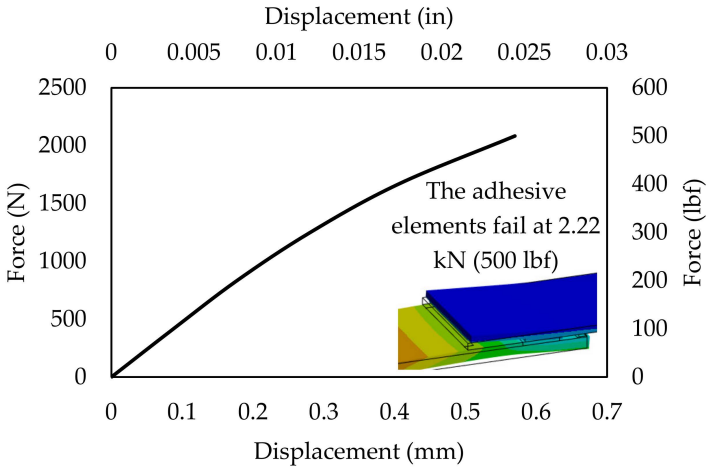

Figure 14. The force-displacement relationship of the load head during the adhesive validation test, as determined through numerical simulations.

2.3.2. Incorporating the Debonding Mechanism into a 12.7 Mm (0.5 inch) Discontinuous IRP System

This section presents the integration of the shear strength of Diglycidyl ether of bisphenol A (DGEBA) epoxy resin, which has been determined to be 20 MPa (2.9 ksi) [25], into the numerical modeling framework of an IRP system subjected to deflection loading. The shear strength value assigned to the DGEBA epoxy adhesive matches with that employed in the experimental tests conducted at the University of Colorado Boulder (CUB). This alignment ensures that the numerical simulations accurately reflect the behaviour of the actual IRP system in the experimental setup at the CUB shown in Figure 1.

The stress results of the IRP system are depicted in Figure 15, while the maximum equivalent stress measured at the midspan of the invert of the IRP alone is depicted in Figure 16. The stress value is measured to be 53.87 MPa (7.81 ksi), which is considerably lower than the maximum allowable stress of 79.42 MPa (13.70 ksi) for the IRP. This observation indicates that the IRP does not experience failure when subjected to the ultimate load of 71.2 kN (16 kip), with a safety factor (SOF) of 1.47. The safety factor represents the ratio of the maximum allowable stress to the actual stress experienced by the IRP, demonstrating that the structure can withstand the applied load with a significant margin of safety. Additionally, Figure 17 provides a visual representation of the progressive debonding process that occurs within the adhesive layer as the applied load increases. It can be observed that the adhesive layer starts to weaken at 28.5 kN (6.4 kip) and experiences substantial debonding at the bottom layer when subjected to the ultimate load of 71.2 kN (16 kip).

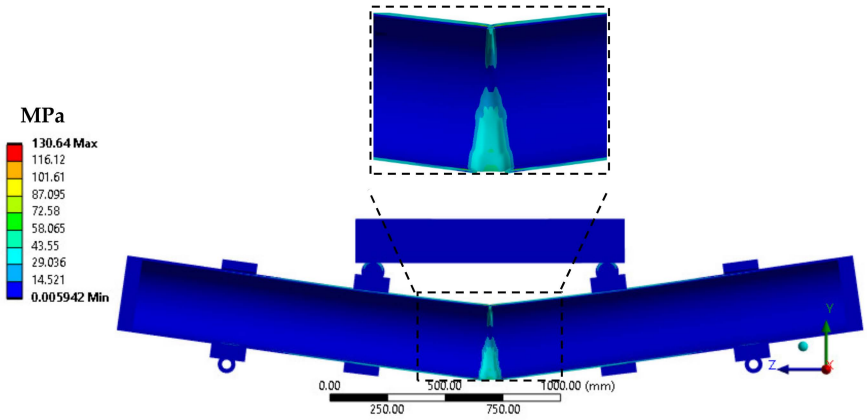

Figure 15. Equivalent stress results of a 12.7 mm (0.5 inch) discontinuous IRP system employing the debonding mechanism at a maximum load of 69.1 kN (15.5 kip) (magnified 29 times).

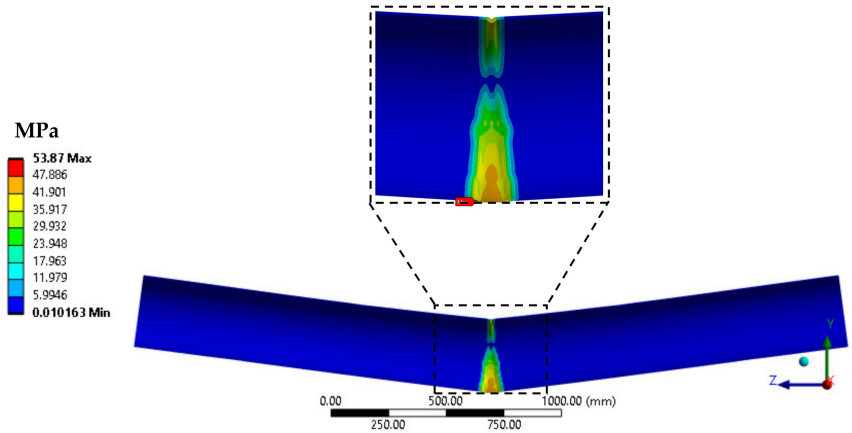

Figure 16. Equivalent stress distribution in the IRP of a 12.7 mm (0.5 inch) discontinuous IRP system employing the debonding mechanism at a maximum load of 69.1 kN (15.5 kip) (magnified 13 times).

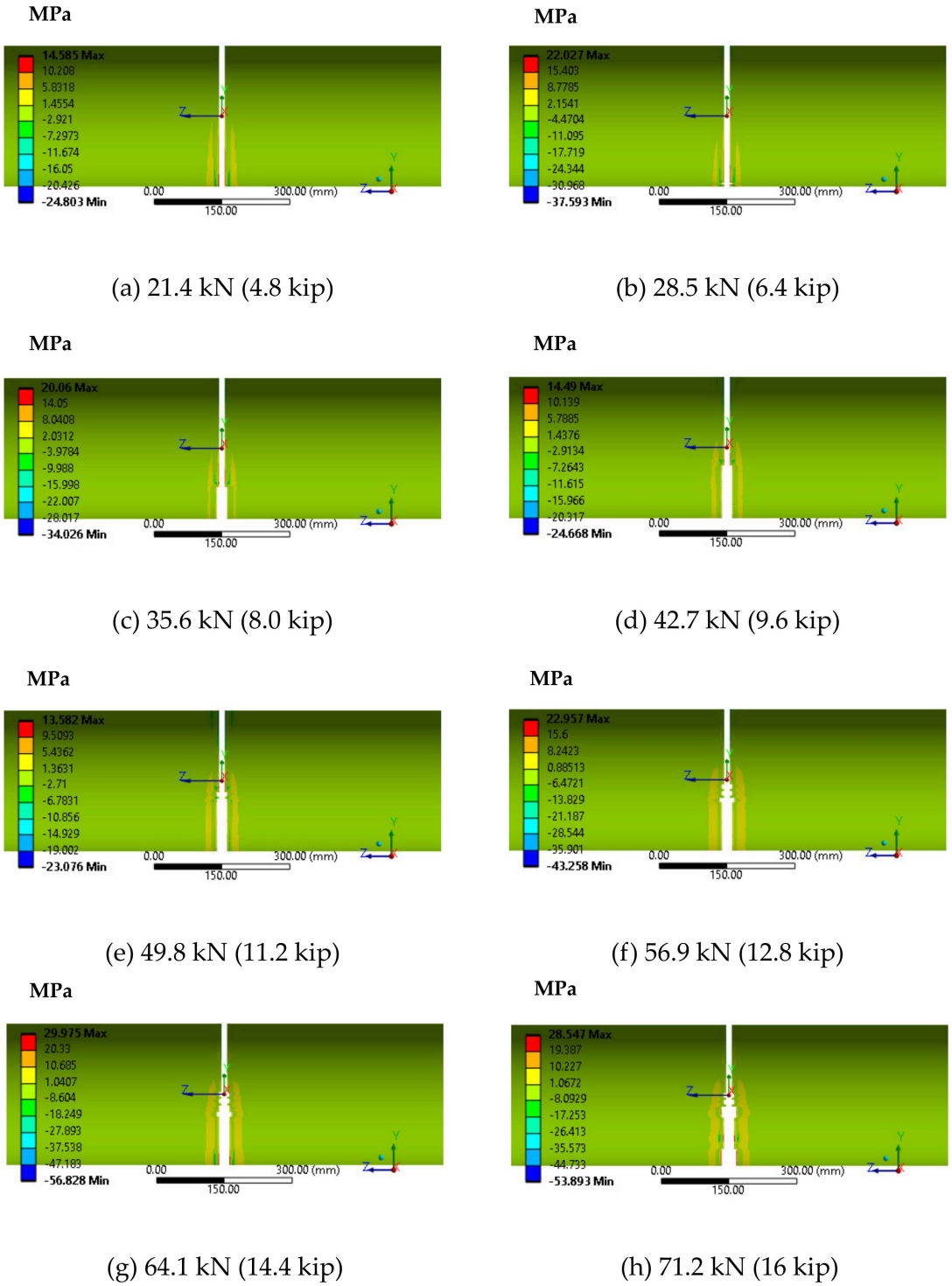

Figure 17. Progressive debonding in the adhesive layer at various load levels for a 12.7 mm (0.5 inch) discontinuous IRP system (true scale).

To further evaluate the effectiveness of incorporating an adhesive layer, Figure 18 and Table 6 present a comprehensive comparison between load versus displacement data obtained from the FEA approach. This incorporates the debonding mechanism in the adhesive layer and the corresponding experimental results from different locations. The outcomes clearly indicate that the inclusion of an adhesive layer significantly improves the agreement between the predicted and experimental results. Specifically, the adhesive layer exhibits a certain level of debonding after reaching approximately 28.5 kN (6.4 kip).

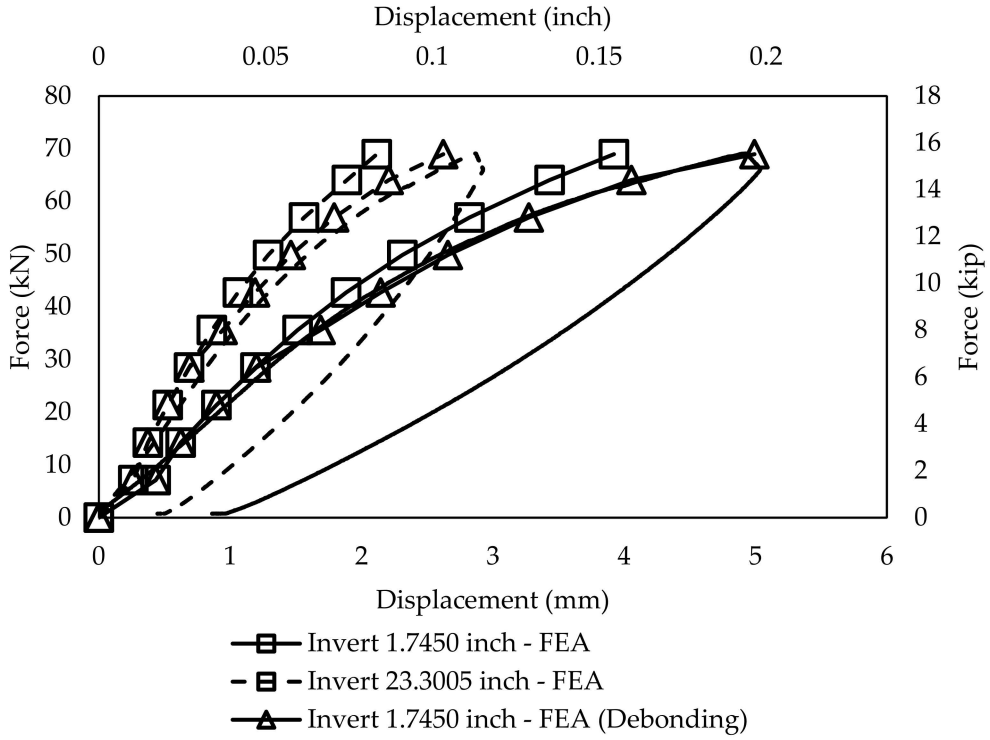

Figure 18. Validation of the load-displacement relationship in the 12.7 mm (0.5 inch) discontinuous IRP system incorporating the debonding mechanism.

Table 6. Comparison of FEA incorporating the debonding mechanism and experimental results for the 12.7 mm (0.5 inch) discontinuous IRP system.

Load kN (kip)	Locations inch	Deflection mm (inch)		Difference(%)
		FEA (Debonding)	Experiment	
21.4 (4.8)	1.7065	0.897 (0.035)	0.975 (0.038)	8
	23.3005	0.526 (0.021)	0.617 (0.024)	15
69.1 (15.5)	1.7065	4.992 (0.197)	4.925 (0.194)	1
	23.3005	2.622 (0.103)	2.855 (0.112)	8

3. Surface Preparation and Its Impact on Debonding

This section examines the influence of adhesive strength on the performance of the IRP system. Different levels of adhesive strength achieved through various preparation techniques on the inner surface of the host pipe before bonding the IRP are investigated. The benchmark shear strength of the adhesive is 20 MPa (2.9 ksi) when the host pipe is freshly cleaned without any specific preparation [25]. In the case of unclean surfaces, the adhesive strength is reduced to 5 MPa (0.7 ksi), while ablated surfaces result in an increased adhesive strength of 40 MPa (5.8 ksi) [25].

3.1. Behaviour of IRP System in 12.7 Mm (0.5 inch) Discontinuous Host Pipe

3.1.1. Deflection Performance

The findings depicted in Figure 19 establish a direct relationship between adhesive strength and the load-bearing capacity of a 12.7 mm (0.5 inch) discontinuous IRP system, highlighting the influence of adhesive strength, which is attributable to surface preparation processes. A higher adhesive strength leads to a better capacity to bear loads because of the higher composite action between the host pipe and the IRP.

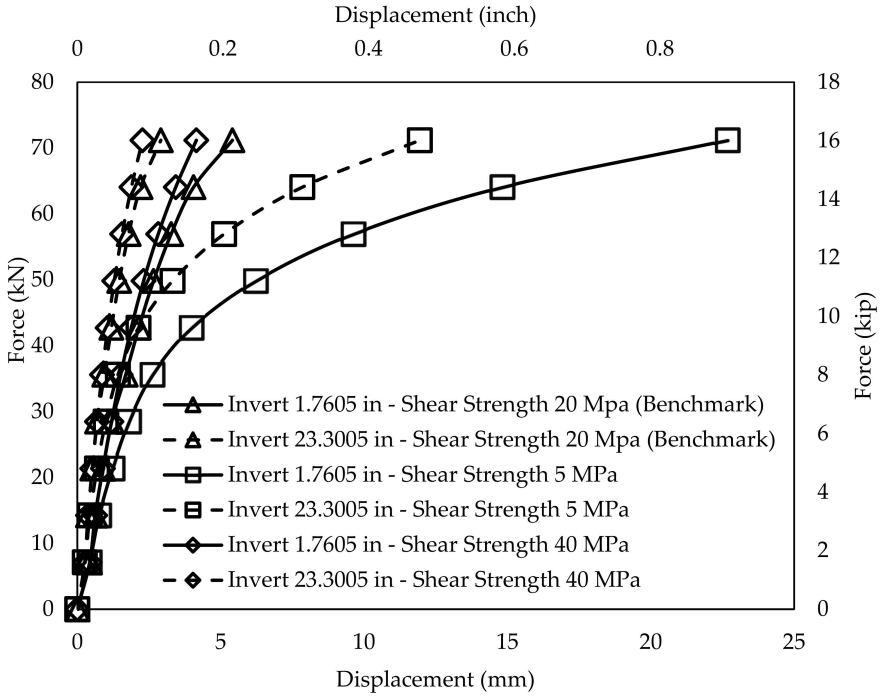

Figure 19. Lateral loading versus deflection of the 0.5 in discontinuous steel IRP system under different levels of adhesive strengths.

Table 7 provides a performance comparison of various adhesive strength levels for a 12.7 mm (0.5 inch) discontinuous IRP system subjected to a 71.2 kN (16 kip) force to explore this relationship further. At the maximum loading of 71.2 kN (16 kip), the unclean surface with a 5 MPa (0.7 ksi) adhesive strength exhibits a deflection of over 310%, while the ablation preparation with a 40 MPa (5.8 ksi) adhesive strength deflects less than 23% compared with the benchmark adhesive strength of 20 MPa (2.9 ksi). The higher the adhesive strength, the lower the likelihood of debonding between the IRP and the host pipe. Consequently, the IRP system could experience a higher level of stress under lateral deformation compared with the system using a lower shear strength adhesive.

Table 7. Performance comparison between various levels of adhesive strength for the 12.7 mm (0.5 inch) discontinuous IRP system at a maximum load of 71.2 kN (16 kip).

Load kN (kip)	Locations inch	Deflection mm (inch)			Difference with Benchmark	
		5 MPa	40 MPa	20 MPa (Benchmark)	5 MPa	40 MPa
71.2 (16)	1.7065	22.682 (0.893)	4.152 (0.164)	5.410 (0.213)	319%↑	23%↓
	23.3005	11.949 (0.470	2.272 (0.089)	2.914 (0.115)	310%↑	22%↓

3.1.2. Debonding Modes of Adhesive Layer

Table 8 demonstrates the different debonding mechanisms observed in three representative cases of the 12.7 mm (0.5 inch) discontinuous IRP system, with varying levels of adhesive strength. These cases were subjected to a fatigue load of 21.4 kN (4.8 kip) and a maximum load of 71.2 kN (16 kip). It is observed that the adhesive with a strength of 20 MPa (2.9 ksi) exhibits failure at a load of 28.5 kN (6.4 kip). In contrast, the adhesive with a strength of 40 MPa (5.8 ksi) remains intact until reaching the maximum load of 71.2 kN (16 kip). On the other hand, the adhesive with a strength of 5 MPa (0.7 ksi) shows early debonding occurring at a load as low as 8.5 kN (1.9 kip).

Table 8. Debonding modes of the various levels of adhesive strengths at a fatigue load of 21.4 kN (4.8 kip) and a maximum load of 71.2 kN (16 kip) for a 12.7 mm (0.5 inch) discontinuous IRP system (true scale).

Adhesive Strength MPa (ksi)	Fatigue Load 21.4 kN (4.8 kip)	Maximum Load 71.2 kN (16 kip)
5 (0.7)	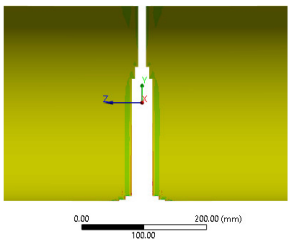	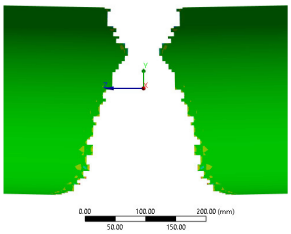
20 (2.9)	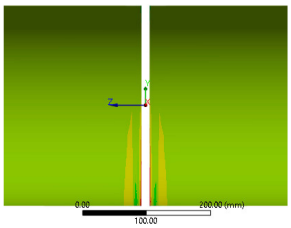	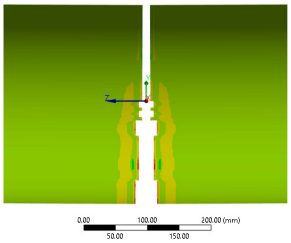
40 (5.8)	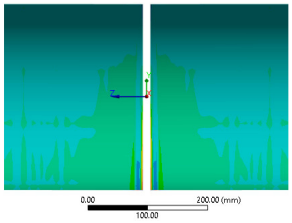	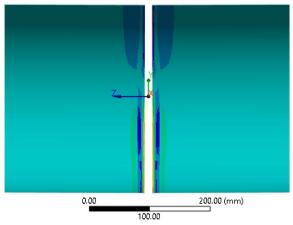

Figure 20 illustrates the average length of debonding in the adhesive layer under a maximum load of 71.2 kN (16 kip) while comparing it across different levels of adhesive shear strength for a 12.7 mm (0.5 inch) discontinuous IRP system. The findings reveal a significantly higher rate of debonding for adhesives with lower shear strengths, with a ratio of 23.6 (slope 1 at 11.8 and slope 2 at 0.5), compared with adhesives with higher shear strengths. When the adhesive strength reaches 20 MPa (2.9 ksi), the debonding of the IRP system is significantly reduced.

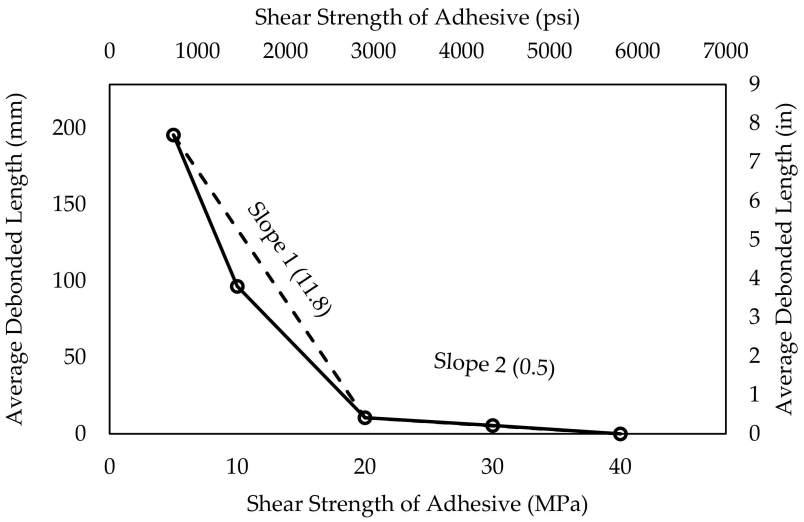

Figure 20. Average debonded length of the adhesive layer at the maximum load of 71.2 kN (16 kip) for 12.7 mm (0.5 inch) discontinuous IRP system versus different levels of adhesive shear strength.

3.1.3. Stress Concentration and Fatigue Life of IRP

Figure 21 illustrates the distribution of normal stress in the IRP layer of a 12.7 mm (0.5 inch) discontinuous IRP system using an adhesive shear strength of 20 MPa (2.9 ksi) under a fatigue load of 21.4 kN (4.8 kip) [26,27]. The case of the shear strength of 20 MPa (2.9 ksi) is chosen as representative for all three levels of shear strength. The results reveal a stress concentration phenomenon at the crack edge on the invert of the IRP, consistent with the findings of previous studies [19,26].

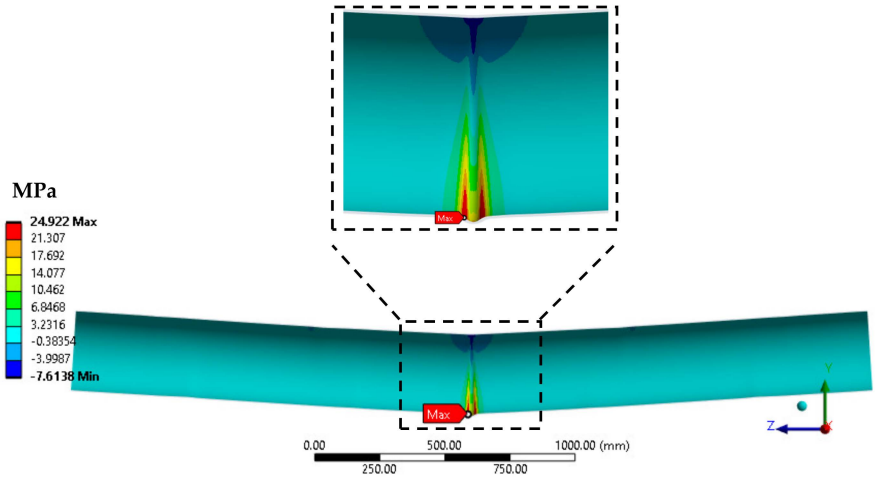

Figure 21. Normal stress results in the longitudinal direction of the IRP layer of a 12.7 mm (0.5 inch) discontinuous IRP system employing the adhesive shear strength of 20 MPa (2.9 ksi) at a fatigue load of 21.4 kN (4.8 kip) (magnified 74 times).

Figure 22 presents a visual representation of the normal stress (axial stress) distribution along the invert line of the IRP of the 12.7 mm (0.5 inch) discontinuous system under a fatigue load of 21.4 kN (4.8 kip) for three different levels of adhesive shear strengths.

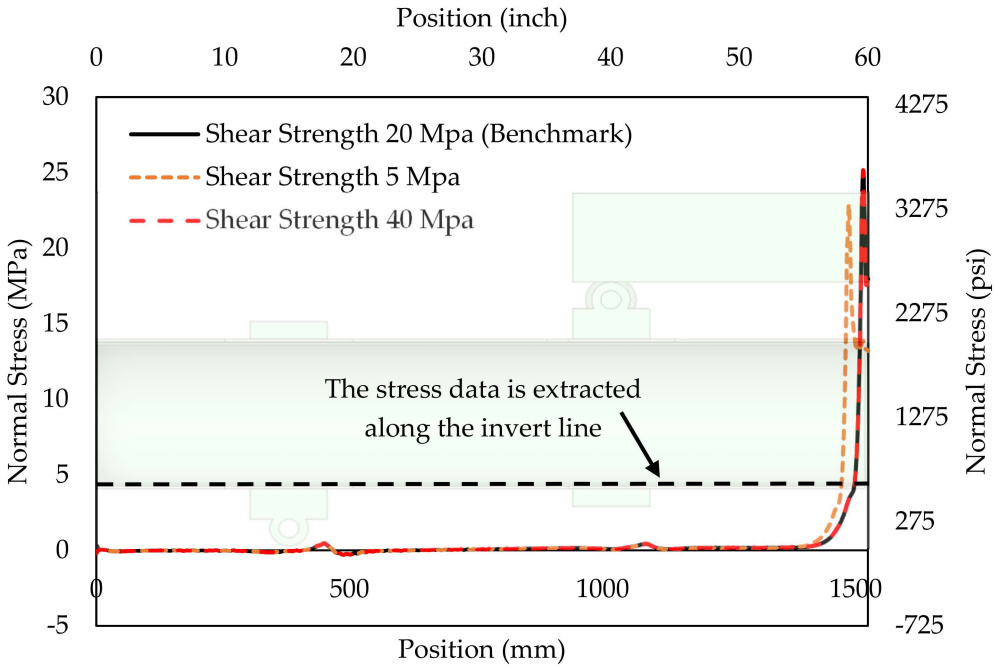

Figure 22. Normal stress distribution in the longitudinal direction of the bottom line of the 12.7 mm (0.5 inch) discontinuous IRP system utilizing the debonding mechanism under a fatigue load of 21.4 kN (4.8 kip).

The fatigue performance of the IRP system was evaluated by integrating the S-N curve for ALTRA10 with the FEA results. The process involved extracting the normal stress concentrations from critical regions, as shown in Figure 22, and mapping them onto the S-N curve presented in Figure 23 [26], which correlates the stress amplitude to the number of cycles to failure for the ALTRA10 material. Table 9 summarizes the minimum life cycles to failure of a 12.7 mm (0.5 inch) discontinuous IRP system with varying levels of adhesive bonding shear strengths. The results indicate that a 12.7 mm (0.5 inch) discontinuous IRP system with 5 MPa (0.7 ksi) adhesive shear strength exhibits a lower stress concentration, consequently leading to a higher life cycle to failure. It is believed that the early debonding of the 5 MPa (0.7 ksi) adhesive at the fatigue load of 21.4 kN (4.8 kip) contributes to stress relief, thus positively affecting the system's durability and longevity. In practice, during fatigue cycling, the debonding near the discontinuity progressively grows larger than the predicted numerical results. These findings in the present numerical results reinforce the experimental findings presented in [15,27–29], which demonstrated that debonding at the separation or discontinuity is a highly desirable characteristic of a well-installed IRP system. By allowing debonding, the IRP can accommodate a certain level of deformation by permitting extra deflection and extension. This ability to strain over a debonded length can prevent premature rupture of the IRP. Figure 24 shows 'before' and 'after' photos of the mechanical aging tests, including 50 years of vehicular traffic (1 million cycles) for the 150 mm (6 inch) nominal diameter cast iron IRP system. It is evident that there was substantial debonding of the IRP from the host pipe in the joint or discontinuity. The debonding occurs within a short distance on either side of the separation, totaling less than one pipe diameter in width.

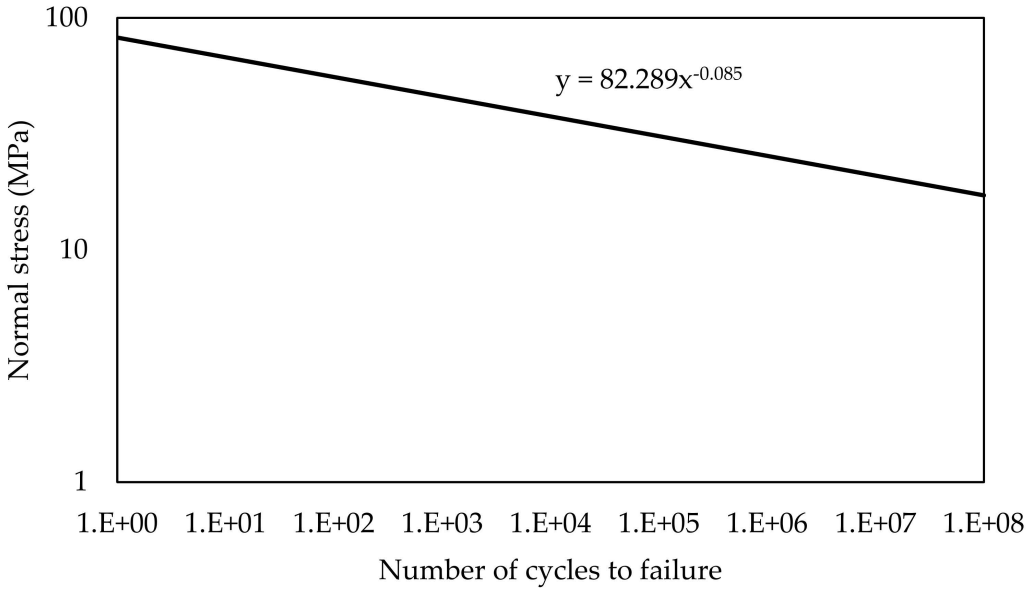

Figure 23. Normal stress versus number of cycles to failure of ALTRA10 IRP [26].

Table 9. Predicted fatigue life of a 12.7 mm (0.5 inch) discontinuous IRP system for various levels of adhesive strength.

Shear Strength MPa	**5**	**20**	**40**
Maximum Normal Stress MPa (ksi)	22.905 (3.322)	24.922 (3.615)	24.922 (3.615)
Predicted Life Cycles to Failure	3,421,786	1,267,786	1,267,786

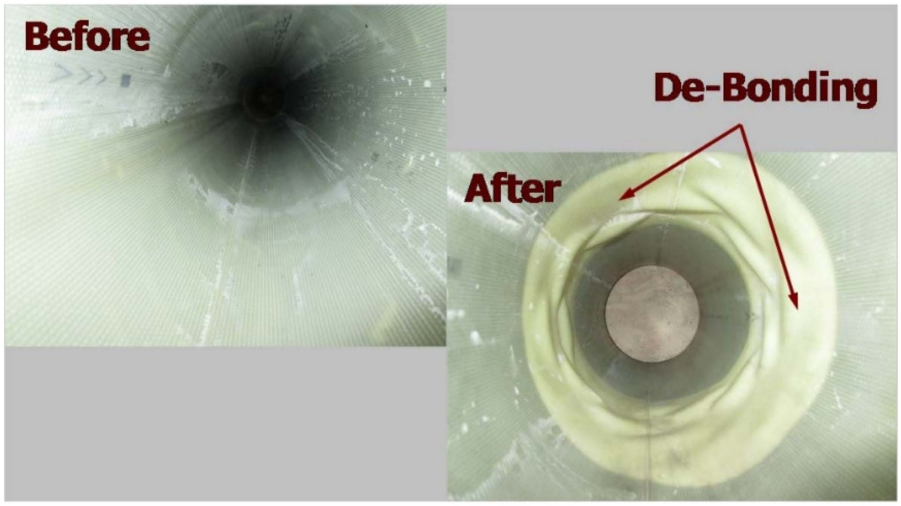

(**a**)

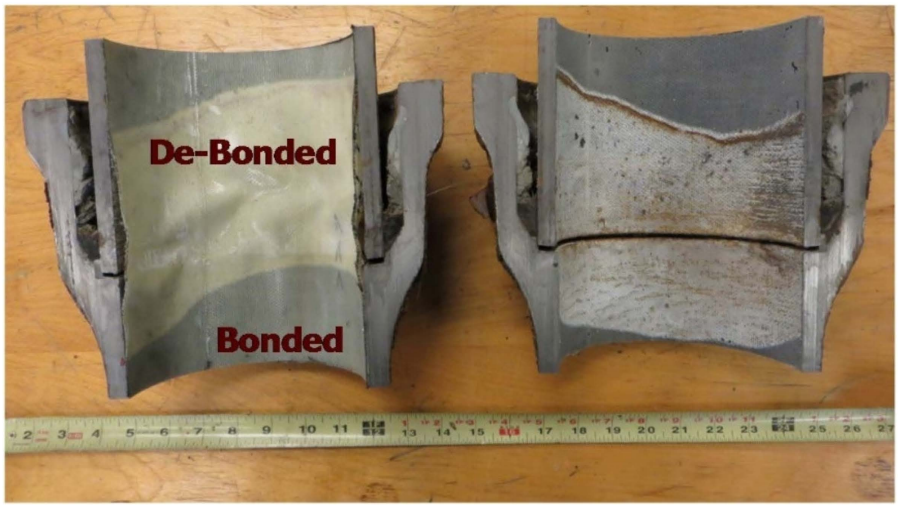

(**b**)

Figure 24. Photos of IRP specimen ′before′ and ′after′ mechanical aging tests: (**a**) internal and (**b**) cut apart joint. Courtesy images from Cornell University [27].

3.1.4. Maximum Stress and Catastrophic Failure

Figure 25 illustrates the distribution of equivalent stress in the IRP layer of a 12.7 mm (0.5 inch) discontinuous IRP system using the representative adhesive shear strength of 20 MPa (2.9 ksi) under a maximum load of 71.2 kN (16 kip). It can be observed that the maximum stress is located at the inverted midspan of the IRP layer at a maximum load of 71.2 kN (16 kip). For small discontinuities in the host pipe and if the load keeps increasing, catastrophic failure may potentially occur because the concentrated stress at the discontinuity edge goes beyond the strength of the IRP. This phenomenon is consistent with the experimental findings from previous studies [15]; therefore, a low level of adhesive strength between the IRP and the host pipe is preferable to facilitate debonding at the discontinuity edge. This relieves stress concentration and, consequently, enables the repair system to withstand higher loads.

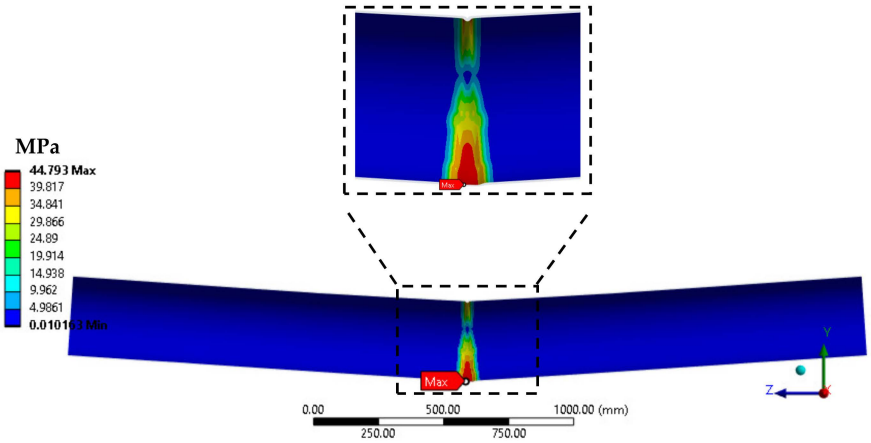

Figure 25. Equivalent stress results of the IRP layer of a 12.7 mm (0.5 inch) discontinuous IRP system employing the adhesive shear strength of 20 MPa (2.9 ksi) at a fatigue load of 71.2 kN (16 kip) (magnified 13 times).

Figure 26 provides a visual representation of the distribution of equivalent stress along the invert line of the IRP under a maximum load of 71.2 kN (16 kip) for various bonding strength scenarios between the host pipe and the IRP. The results show that the maximum equivalent stress is 41.781 MPa (6.060 ksi) for 5 MPa (0.7 ksi) shear strength, 44.793 MPa (6.497 ksi) for 20 MPa (2.9 ksi) shear strength, and 47.166 MPa (6.841 ksi) for the highest shear strength of 40 MPa (5.8 ksi). This indicates that there will be no potential material failure in any of the cases, as the maximum stresses are significantly lower than the strength of the ALTRA10, which is 79.420 MPa (11.519 ksi). Furthermore, it can be observed that under the maximum load, the lower the adhesive shear strength, the lower the maximum stress yield in the IRP. It can be inferred, therefore, that debonding occurs in the scenarios of 5 MPa (0.7 ksi) and 20 MPa (2.9 ksi), which helps alleviate stress over a more extended free length of the IRP.

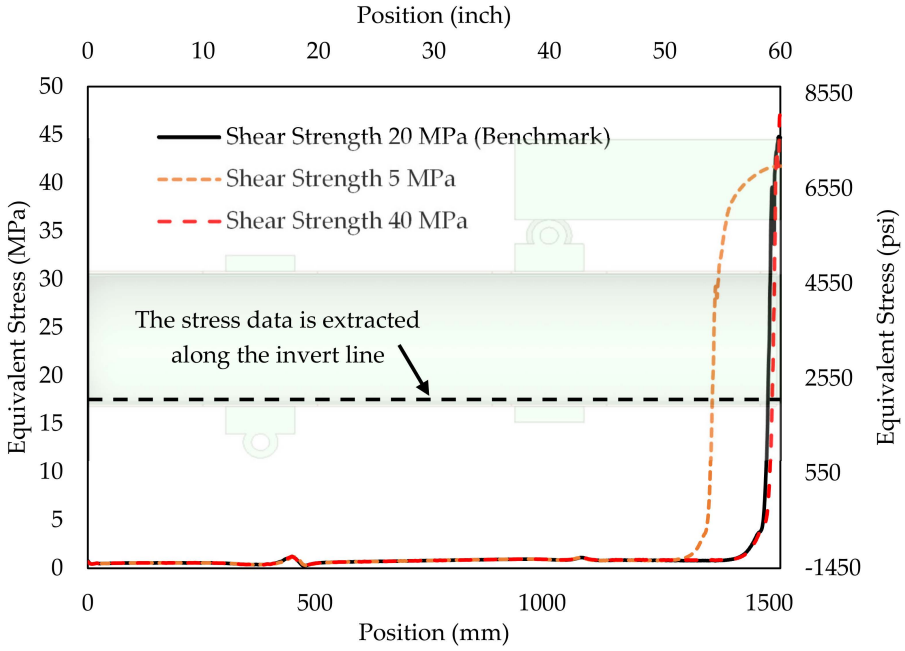

Figure 26. Equivalent stress distribution in the longitudinal direction of the bottom line of the 12.7 mm (0.5 inch) discontinuous IRP system utilizing the debonding mechanism under a maximum load of 71.2 kN (16 kip).

3.2. Behaviour of IRP System in 152.4 Mm (6 inch) Discontinuous Host Pipe

This section investigates how the adhesive layer affects the behavior of an IRP system within a host pipe featuring a 152.4 mm (6 inch) wide circumferential gap. This study commences with the preparation of the ablated surface within the host pipe, exhibiting an adhesive strength of 40 MPa (5.8 ksi), to determine the maximum load capacity for the broader discontinuity system. Figure 27 depicts the stress response of the 152.4 mm (6 inch) discontinuous IRP system when subjected to 80% of the full load (71.2 kN or 16 kip) utilized for the 12.7 mm (0.5 inch) discontinuous IRP system, which is equivalent to 56.9 kN (12.8 kip). It is observed that when the applied force exceeds 56.9 kN (12.8 kip), the 152.4 mm (6 inch) discontinuity width IRP system experiences local deformation failure on the crown of the discontinuity section. To maintain simplicity, the load of 56.9 kN (12.8 kip) is defined as the maximum applied load for the 152.4 mm (6 inch) discontinuous IRP system while considering various levels of adhesive strengths resulting from different surface preparation methods before bonding the host pipe and the IRP system.

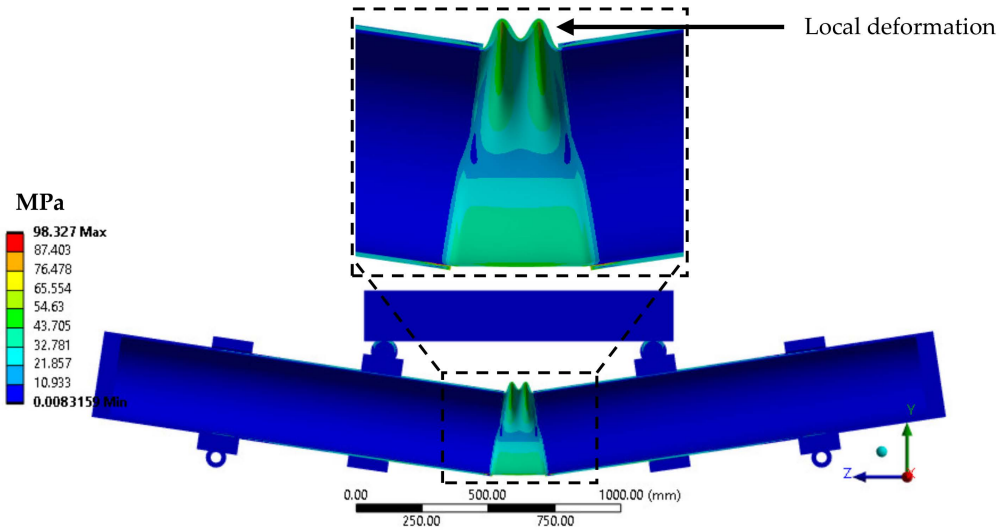

Figure 27. Equivalent stress results of a 152.4 mm (6 inch) discontinuous IRP system employing the adhesive shear strength of 40 MPa (5.8 ksi) at a load of 56.9 kN (12.8 kip) (magnified 7.2 times).

3.2.1. Deflection Performance

Figure 28 illustrates the load versus deflection behavior of the IRP in a host pipe with 152.4 mm (6 inch) wide discontinuity, offering valuable insights into its mechanical response under different levels of adhesive shear strengths. Table 10 compares the performance of the 152.4 mm (6 inch) IRP system at a load of 56.9 kN (12.8 kip) for different levels of adhesive strength. The results reveal that the unclean surface, with an adhesive strength of 5 MPa (0.7 ksi), experiences 20% more deflection, whereas the ablated preparation, with an adhesive strength of 40 MPa (5.8 ksi), exhibits a deflection of less than 16% when compared with the benchmark adhesive strength of 20 MPa (2.9 ksi). It is evident that the 152.4 mm (6 inch) IRP system is much less affected by changes in adhesive strength compared with the 12.7 mm (0.5 inch) IRP system, as highlighted in Table 7. This behavior can be explained by the relatively wide discontinuity of 152.4 mm (6 inches), resulting in a lower overall bending stiffness and allowing for better absorption of deflection compared with the shorter circumferential discontinuity of 12.7 mm (0.5 inches); therefore, it could leverage the deflection change with respect to adhesive bonding change. The behavior can also be observed in Figure 29.

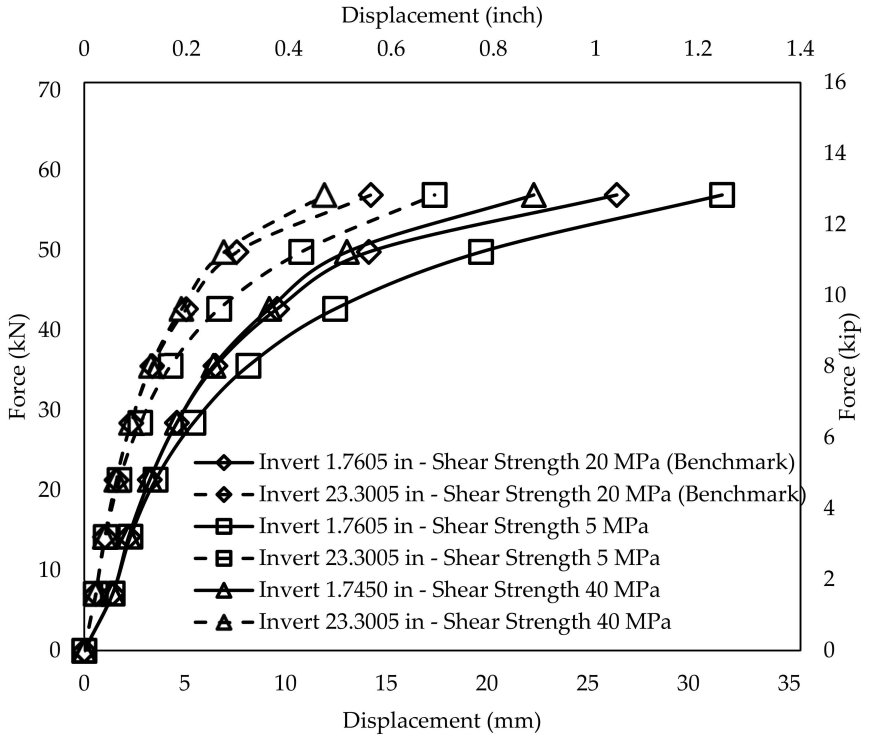

Figure 28. Lateral loading versus deflection of the 152.4 mm (6 inch) discontinuous IRP system under different levels of adhesive strengths.

Table 10. Performance comparison between various levels of adhesive strength for the 152.4 mm (6 inch) discontinuous IRP system at a load of 56.9 kN (12.8 kip).

Load kN (kip)	Locations inch	Deflection mm (inch)			Difference with Benchmark	
		5 MPa	40 MPa	20 MPa (Benchmark)	5 MPa	40 MPa
56.9 (12.8)	1.7065	31.671 (1.247)	22.323 (0.879)	26.441 (1.041)	20%↑	16%↓
	23.3005	17.400 (0.685)	11.926 (0.470)	14.234 (0.560)	22%↑	16%↓

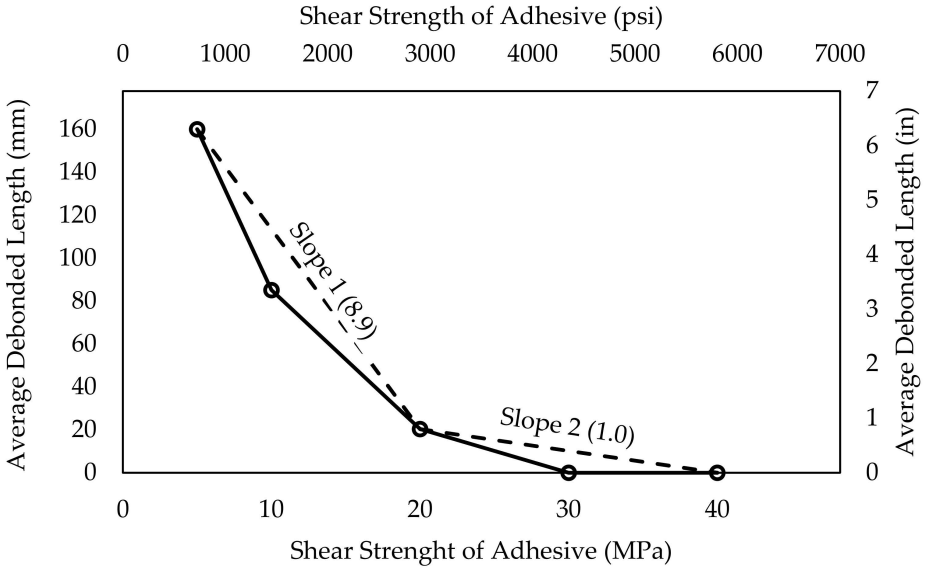

Figure 29. Average debonding length of the adhesive layer at the maximum load of 56.9 kN (12.8 kip) for 152.4 mm (6 inch) discontinuous IRP system versus different levels of adhesive shear strength.

3.2.2. Debonding Modes of Adhesive Layer

Table 11 provides an overview of the debonding modes observed in the adhesive layer under varying loading levels and shear strengths of the adhesive. At the fatigue load, it was found that the 5 MPa (0.7 ksi) adhesive strength exhibited minor debonding. However, for the stronger adhesive strengths of 20 MPa (2.9 ksi) and 40 MPa (5.8 ksi), no debonding was observed. Under the maximum load, significant debonding was observed for the adhesive layer with 5 MPa (0.7 ksi) strength. In contrast, the adhesive layer with 20 MPa (2.9 ksi) strength showed moderate debonding. Remarkably, the adhesive layer with the highest shear strength of 40 MPa (5.8 ksi) remained intact without any observable debonding.

Table 11. Debonding modes of the various levels of adhesive strengths at a fatigue load of 21.4 kN (4.8 kip) and a maximum load of 56.9 kN (12.8 kip) for a 152.4 mm (6 inch) discontinuous IRP system (true scale).

Adhesive Strength MPa (ksi)	Fatigue Load 21.4 kN (4.8 kip)	Maximum Load 56.9 kN (12.8 kip)
5 (0.7)	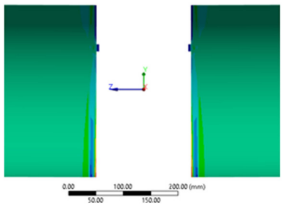	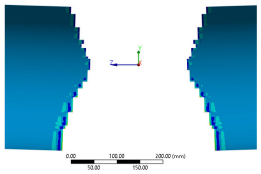
20 (2.9)	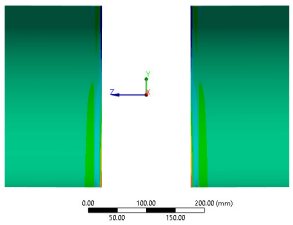	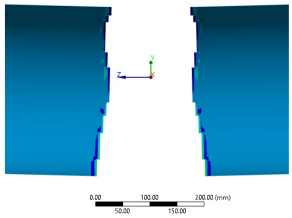
40 (5.8)	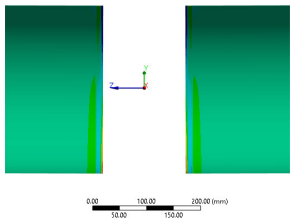	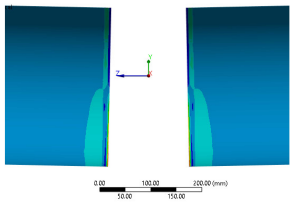

Figure 29 illustrates the average debonded length of the adhesive layer at the maximum load of 56.9 kN (12.8 kip), comparing the debonded lengths across different levels of adhesive shear strength for the case of a 152.4 mm (6 inch) discontinuous system. The results show a substantially higher debonding rate associated with lower adhesive shear strengths compared with higher ones, with a ratio of 8.9 (slope 1 at 8.9 and slope 2 at 1.0), indicating that a decrease in adhesive shear strength results in increased debonding within the adhesive layer. Additionally, it is observed that there are no tangible benefits from excessively high shear strengths of the adhesive, as they do not significantly contribute to the bonding/debonding mechanism. For instance, no debonding is observed in adhesives with shear strengths exceeding 30 MPa (4.4 ksi).

3.2.3. Stress Concentration and Fatigue Life of IRP

Similar to a 12.7 mm (0.5 inch) discontinuous IRP system, a 152.4 mm (6 inch) discontinuous IRP system exhibits a stress concentration at the crack edge on the invert of the IRP, as shown in Figure 30. However, the ratio between the concentrated stress at the crack and the midspan stress is higher for the 12.7 mm (0.5 inch) discontinuous case, i.e., 1.39, in comparison with 1.12 for the 152.4 mm (6 inch) discontinuous system as shown in Figure 22 and Figure 31, respectively. These findings indicate that the 12.7 mm (0.5 inch) IRP system

experiences a more pronounced stress concentration at the crack edge than the 152.4 mm (6 inch) IRP system. This behavior can be explained by the relatively wide discontinuity of 152.4 mm (6 inches), which allows for better absorption of stress concentration compared with the shorter discontinuity of 12.7 mm (0.5 inches). It is also observed that the shear strength levels of the adhesive layer have little effect on the magnitude of normal stress for the 152.4 mm (6 inch) discontinuous system.

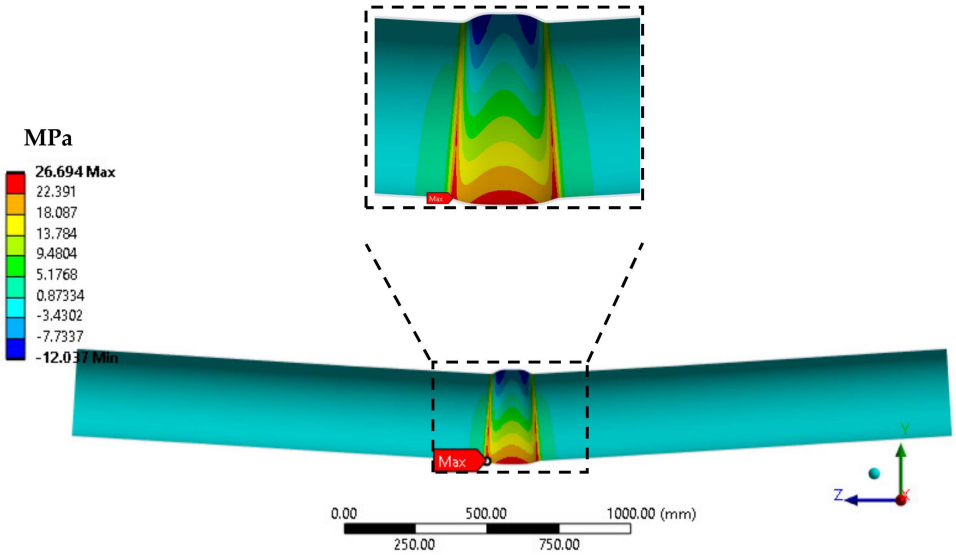

Figure 30. Normal stress results in the longitudinal direction of the IRP layer of a 152.4 mm (6 inch) discontinuous IRP system employing the adhesive shear strength of 20 MPa (2.9 ksi) at a fatigue load of 21.4 kN (4.8 kip) (magnified 23 times).

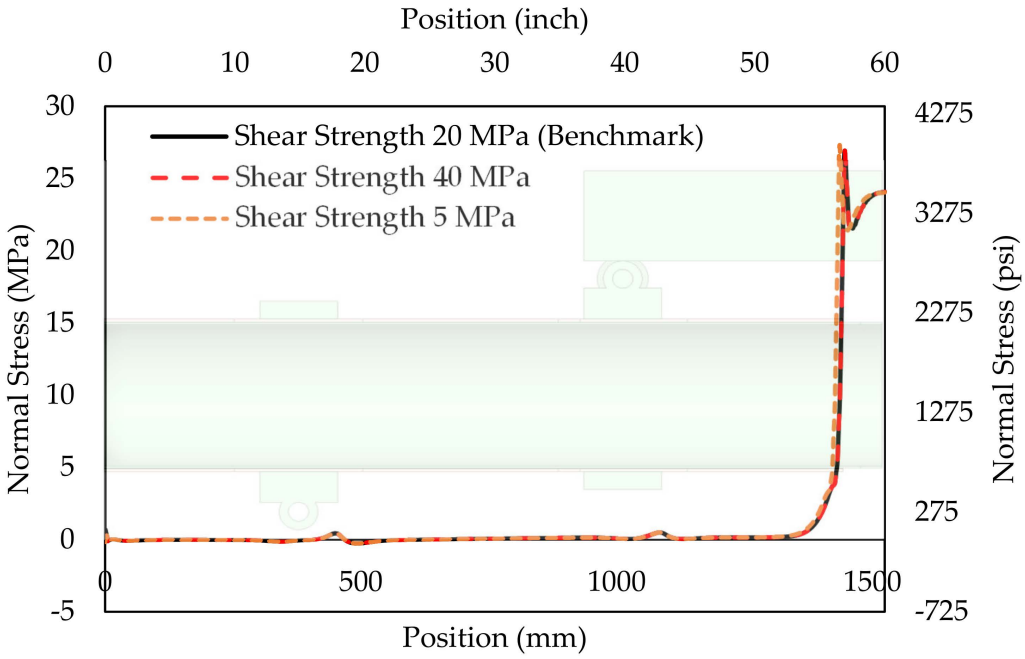

Figure 31. Normal stress distribution in the longitudinal direction of the bottom line of the 12.7 mm (0.5 inch) discontinuous IRP system utilizing the debonding mechanism under a fatigue load of 21.4 kN (4.8 kip).

Under fatigue, the 152.4 mm (6 inch) discontinuous system exhibits similar concentration stresses in all three cases: 27.308 MPa (3.961 ksi) for a 5 MPa (0.7 ksi) shear strength and 26.924 MPa (3.095 ksi) for both 20 MPa (2.9 ksi) and 40 MPa (5.8 ksi) shear strengths. These

levels of concentration stresses are higher than those observed in the 12.7 mm (0.5 inch) discontinuous IRP system, resulting in lower life cycles, as shown in Table 12: 432,419 cycles for 5 MPa (0.7 ksi) shear strength and 510,812 cycles for both 20 MPa (2.9 ksi) and 40 MPa (5.8 ksi) shear strength. These fatigue cycles fall short of 1 million cycles, which is required to demonstrate the 50-year design life of the pipeline repair system. To enhance the fatigue life of the 152.4 mm (6 inch) discontinuous IRP system while maintaining the material property, a thicker IRP layer should be employed. It can be explained that the 152.4 mm (6 inch) discontinuous system experiences a higher magnitude of stress concentration compared with the 12.7 mm (0.5 inch) discontinuous IRP system due to the elevated level of deformation.

Table 12. Predicted fatigue life of a 152.4 mm (6 inch) discontinuous IRP system for various levels of adhesive strength.

Shear Strength MPa	**5**	**20**	**40**
Maximum Normal Stress MPa (ksi)	27.308 (3.961)	26.924 (3.095)	26.924 (3.095)
Predicted life cycles to failure	432,419	510,812	510,812

3.2.4. Maximum Stress and Failure Mechanism

Figures 32–34 present the stress distribution in the IRP layer for a 152.4 mm (6 inch) discontinuous system with various adhesive shear strengths, loaded to a maximum of 56.9 kN (12.8 kip). The analyses indicate that the local deformation phenomenon primarily occurs at the crown of the IRP for all cases. This critical deformation point could potentially lead to a catastrophic failure of the system under loads of approximately 56.9 kN (12.8 kip) or higher. Although lower shear strength adhesives tend to cause more debonding, as shown in Table 11, they have a negligible effect on the failure of the IRP under the maximum load. Local deformation mainly occurs at the crown of the IRP midspan. To improve the local deformation bearing capability, it may be considered to use a thicker IRP for the 152.4 mm (6 inch) discontinuity to increase the bending stiffness of the system.

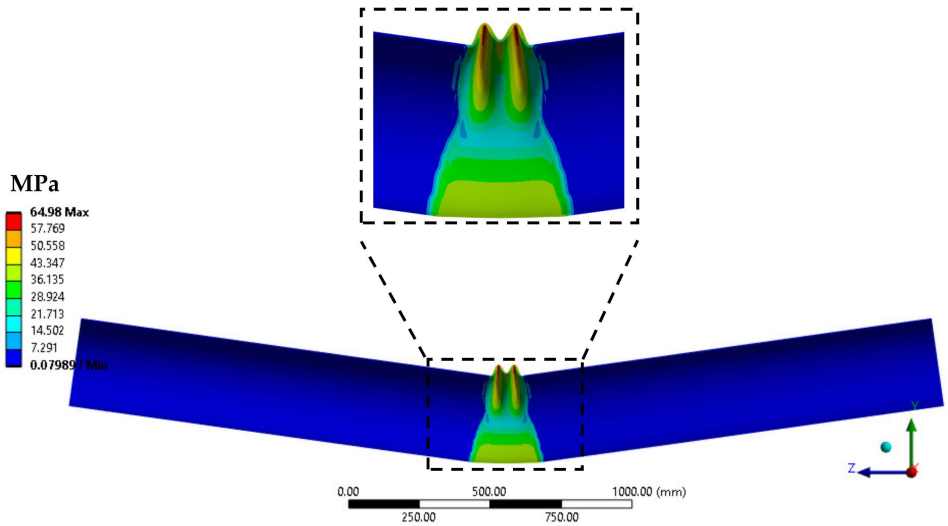

Figure 32. Equivalent stress results in the IRP layer of a 152.4 mm (6 inch) discontinuous IRP system employing the adhesive shear strength of 20 MPa (2.9 ksi) at a maximum load of 56.9 kN (12.8 kip) (magnified 5.6 times).

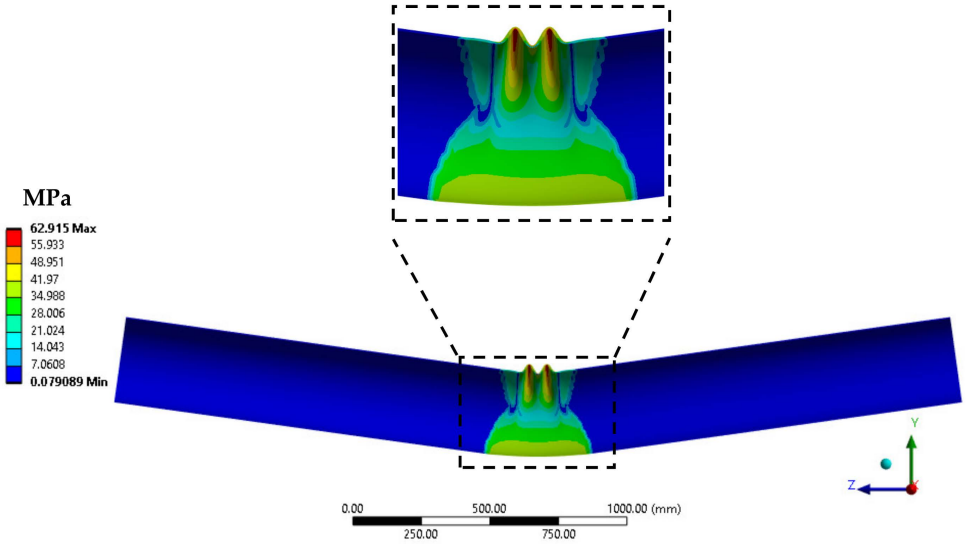

Figure 33. Equivalent stress results in the IRP layer of a 152.4 mm (6 inch) discontinuous IRP system employing the adhesive shear strength of 5 MPa (0.7 ksi) at a maximum load of 56.9 kN (12.8 kip) (magnified 4.5 times).

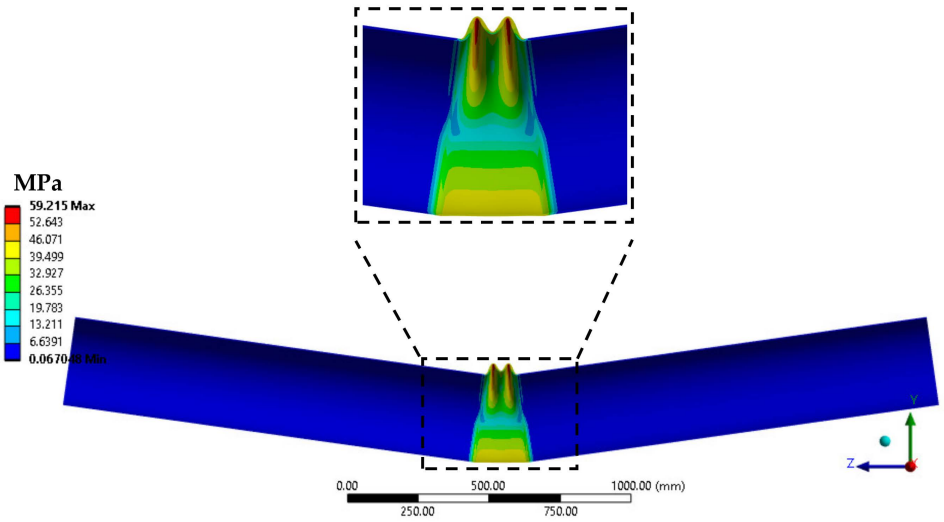

Figure 34. Equivalent stress results in the IRP layer of a 152.4 mm (6 inch) discontinuous IRP system employing the adhesive shear strength of 40 MPa (5.8 ksi) at a maximum load of 56.9 kN (12.8 kip) (magnified 6.6 times).

A similar experimental setup was employed, utilizing the ALTRA10 and a 152.4 mm (6 inch) discontinuous host pipe. This arrangement was positioned in a four-point bending configuration measuring 26 inches by 40 inches by 26 inches. Prior to data collection, it was reported that the system underwent several loading cycles, as shown in Figure 1. This preliminary loading revealed comparable deflection behavior and local deformation failure, as depicted in Figure 35. Local deformation failure was observed both at the crown midspan of the IRP layer under a load of 54.7 kN (12.3 kip), resulting in a deflection of 33.858 mm (1.333 inches) at the invert midspan. The obtained FEA results and experimental findings exhibited substantial agreement, particularly concerning the local deformation outcomes. Specifically, FEA indicated a local deformation load of 56.9 kN (12.8 kip), whereas the experimental result was 54.7 kN (12.3 kip), yielding a difference of 4.065%.

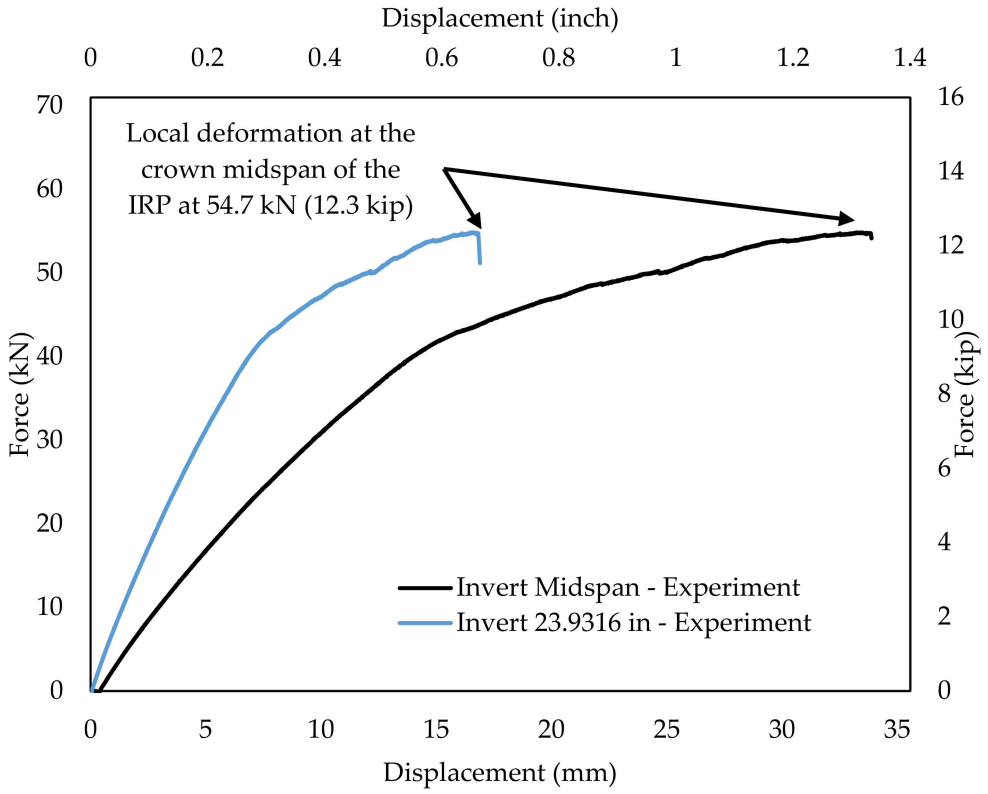

Figure 35. Local deformation failure in the IRP layer of a 152.4 mm (6 inch) discontinuous IRP system at a maximum load of 54.7 kN (12.3 kip). Courtesy data from the University of Colorado Boulder.

3.3. Continuous IRP System with Different Levels of Adhesive Strength

This section presents an analysis of the deflection performance, debonding mode of the adhesive layer, fatigue life, and catastrophic failure of the continuous steel IRP system under deflection loading ranging from a fatigue load of 21.4 kN (4.8 kip) to a maximum of 71.2 kN (16 kip). The numerical findings indicate that the system remains intact, with no observed debonding or failure in both the adhesive and IRP layers across a range of shear strengths from 5 MPa (0.7 ksi) to 40 MPa (5.8 ksi), even when loaded up to a maximum of 71.2 kN (16 kip). Therefore, the continuous system exhibits better strength and significantly smaller deflection compared with the discontinuous ones due to the higher level of overall stiffness [16].

3.3.1. Deflection Performance

Figure 36 compares the deflection performance of the three IRP systems, including the continuous, 12.7 mm (0.5 inch), and 152.4 mm (6 inch) discontinuous configurations for the specific case of a 20 MPa (2.9 ksi) shear strength on the adhesive. It can be observed that the continuous IRP yields higher strength and, therefore, lower deflection compared with the other two discontinuous systems. Specifically, at the maximum load of 71.2 kN (16 kip) for the location of invert 591.833 mm (23.3005 inches), the continuous IRP system exhibits a deflection of 0.543 mm (0.021 inches), while the 12.7 mm (0.5 inch) discontinuous IRP system shows a deflection of 5.410 mm (0.213 inches), and the 152.4 mm (6 inch) discontinuous IRP system exhibits a deflection of 26.442 mm (1.041 inches).

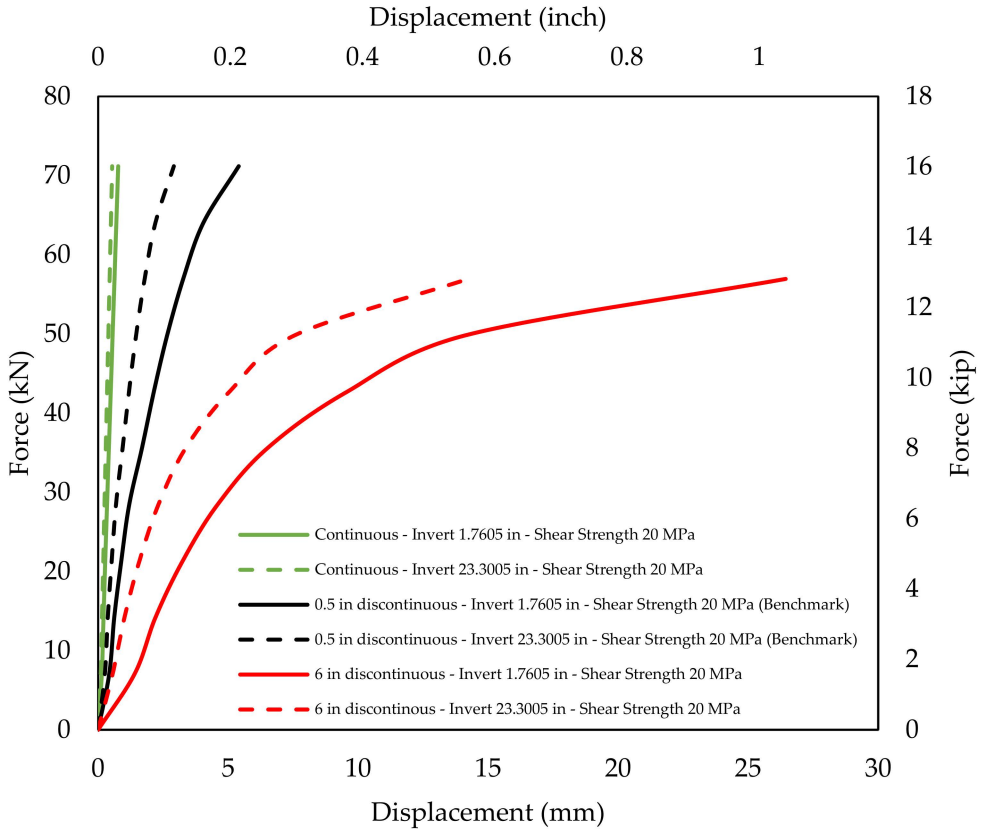

Figure 36. Lateral loading versus deflection of the three IRP systems: continuous, 12.7 mm (0.5 inch), and 152.4 mm (6 inch) discontinuous.

3.3.2. Debonding Modes of Adhesive Layer

Figure 37 illustrates the shear stress distribution in the adhesive layer of a continuous IRP system subjected to a load of 71.2 kN (16 kip). The results indicate that the maximum shear stress observed in the adhesive layer is only 0.189 MPa (0.027 ksi), which is significantly lower than the lowest shear strength of 5 MPa (0.7 ksi) for the unprepared surface. As a result, no debonding is observed in the adhesive layer, even under the maximum load of 71.2 kN (16 kip) in the continuous IRP system.

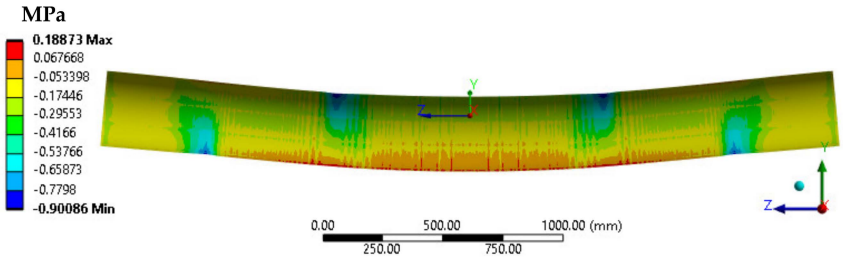

Figure 37. Shear stress results in the adhesive layer of a continuous IRP system employing the adhesive shear strength of 20 MPa (2.9 ksi) at a maximum load of 71.2 kN (magnified 98 times).

3.3.3. Stress Concentration and Fatigue Life of IRP

Figure 38 shows the normal stress distribution in the IRP in a continuous host pipe when subjected to a fatigue load of 21.4 kN (4.8 kip). As there is no discontinuity in the host pipe, no concentrated stress is observed in the midspan region, and the maximum normal stress is very small, approximately 0.267 MPa (0.039 ksi). This stress level ensures almost infinite life cycles when using the SN curve displayed in Figure 23.

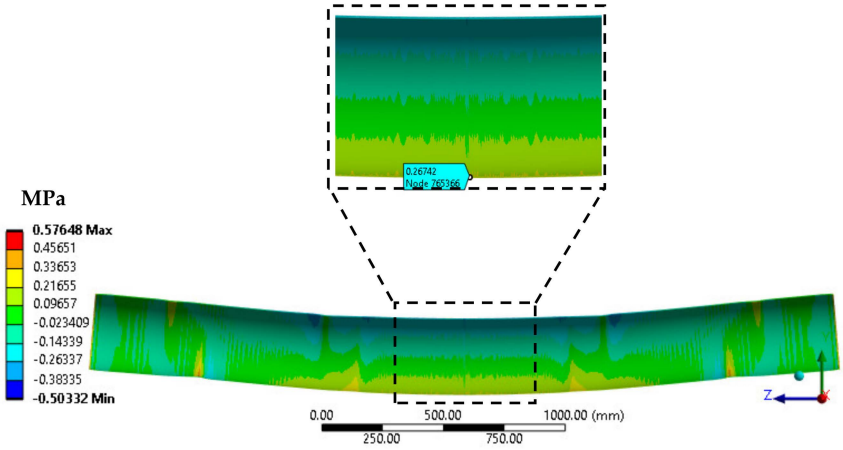

Figure 38. Normal stress results in the IRP layer of a continuous IRP system employing the adhesive shear strength of 20 MPa (2.9 ksi) at a fatigue load of 71.2 kN (magnified 270 times).

3.3.4. Maximum Stress and Failure Mechanism

Figure 39 illustrates the equivalent stress distribution in the IRP of a continuous host pipe when subjected to a maximum load of 71.2 kN (16 kip). It can be observed that the maximum stress in the midspan region is approximately 1.106 MPa (0.160 ksi), which is well below the strength of ALTRA10 at 79.420 MPa (11.519 ksi). This indicates that the IRP does not experience any material failure or debonding from the host pipe under a maximum load of 71.2 kN (16 kip). This result suggests that debonding and material failure may not be significant concerns for an IRP within a continuous host pipe, but they become critical factors when it is used as a repair system in a pipeline with circumferential discontinuity.

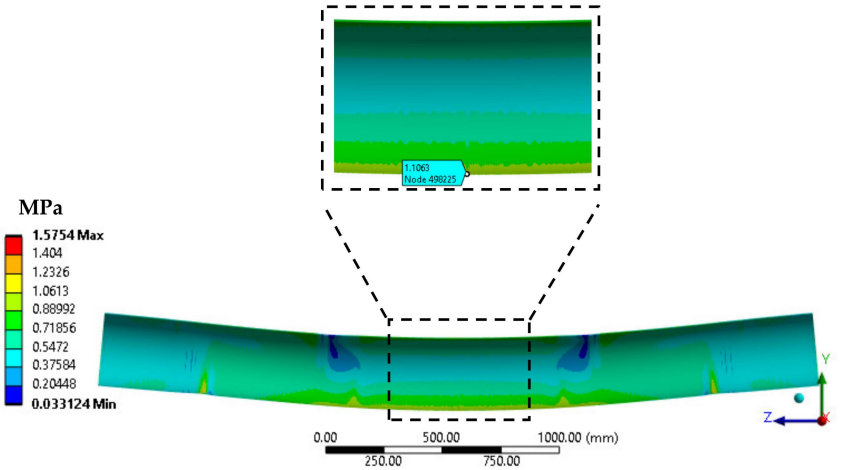

Figure 39. Equivalent stress results in the IRP layer of a continuous IRP system employing the adhesive shear strength of 20 MPa (2.9 ksi) at a maximum load of 71.2 kN (16 kip) (magnified 98 times).

4. Conclusions

A comprehensive numerical investigation was conducted to evaluate the performance of internal replacement pipes (IRPs) under deflection loading, considering various configurations and inside surface preparations of the host pipe. Through the development and validation of an advanced numerical method using the full-scale four-point bending physical test results and shear strength criteria of the adhesive layer, this study yields valuable insights into the behavior of the IRP system. The key findings of the investigation are as follows:

- The adhesive shear strength should be considered in numerical analyses of the nonlinear behavior of the IRP system under lateral deformation. A deviation of only 1% was observed between the results of the numerical analysis and the full-scale experiment. This deviation can be as high as 20% when the IRP is assumed to be fully bonded to the host pipe.
- Debonding of the IRP in a host pipe with a 12.7 mm (0.5 inch) circumferential discontinuity can lead to increased deflection but reduced stress concentration near the discontinuity edge, thus improving the life cycle of the repair system.
- For systems featuring a 12.7 mm (0.5 inch) crack width, the critical point of potential failure was observed at the invert midspan of the IRP layer, while large discontinuous systems with a 152.4 mm (6 inch) discontinuity width exhibited potential local deformation at the crown midspan of the IRP layer, particularly under excessively large loads.
- The strength of the adhesive or surface preparation methods does not significantly impact the deflection or fatigue performance of the IRP system in a host pipe with a 152.4 mm (6 inch) or half discontinuity or half the host pipe diameter. This can be due to the stress absorption capability of such a wide discontinuity.
- The adhesive shear strength and surface preparation have a negligible effect on the performance of the continuous IRP system in terms of load-bearing capacity, fatigue, and catastrophic failure, attributable to the higher level of overall stiffness.
- It is crucial to select adhesives with a minimum level of shear strength while also considering the necessary debonding length. This ensures that small discontinuities are managed effectively, promoting improved fatigue life for the system.
- A balance of adhesive strength and debonding length is necessary to maintain the fatigue life of the IRP system without adverse effects. Excessive bonding might be detrimental. Typically, the maximum shear strength for adhesive or debonding length is determined through analysis, ensuring it does not compromise fatigue life.

The successful validation of the numerical approach against analytical solutions and experimental data with high accuracy reinforces confidence in the fidelity of the findings. This enhanced numerical method using maximum stress failure criteria, along with the insights gained from this study, can serve as a valuable resource for future research in the field of pipe-in-pipe studies. While the primary focus of this work is on lateral deflection, the current approach can also be applied to other performance objectives, such as axial deformation and parallel compression. Moreover, the guidelines derived from this investigation can aid in the design and maintenance phases of trenchless IRP technology, contributing to more efficient and robust pipeline repair systems.

Although the FEA results align well with both analytical and experimental data, further refinement of the FEA model is an ongoing effort. One potential improvement is the calibration of the adhesive layer thickness, which is currently limited by the element aspect ratio. Optimizing this parameter could enhance the accuracy of the numerical results while maintaining computational efficiency, and it presents a promising area for future research.

Author Contributions: Conceptualization, T.C.M.T., A.M. and B.P.W.; methodology, T.C.M.T.; software, T.C.M.T.; validation, T.C.M.T. and P.D.; formal analysis, T.C.M.T.; investigation, T.C.M.T., P.D., A.M. and B.P.W.; resources A.M. and B.P.W.; data curation, T.C.M.T. and P.D.; writing—original draft preparation, T.C.M.T.; writing—review and editing, T.C.M.T., A.M., P.D., B.P.W. and W.K.; visualization, H.A., S.K. and A.S.; supervision, A.M.; project administration, A.M. and B.P.W.; funding acquisition, B.P.W. All authors have read and agreed to the published version of the manuscript.

Funding: The information, data, or work presented herein was funded in part by the Advanced Research Projects Agency-Energy (ARPA-E), U.S. Department of Energy, under Award Number DE-AR0001327. The views and opinions of the authors expressed herein do not necessarily state or reflect those of the Department of Energy (DOE) or the Advanced Research Projects Agency-Energy (ARP-E).

Data Availability Statement: The original contributions presented in the study are included in the article, further inquiries can be directed to the corresponding author.

Conflicts of Interest: The authors declare no conflict of interest.

References

1. International Energy Agency (IEA). Natural Gas 2021. Available online: https://www.iea.org/reports/global-energy-review-2021/natural-gas (accessed on 9 May 2023).
2. U.S. Department of Energy. *Monthly Energy Review April 2023*; U.S. Energy Information Administration, Office of Energy Statistics, U.S. Department of Energy: Washington, DC, USA, 2023.
3. Australian Government. *Australian Energy Update 2022*; Department of Climate Change, Energy, the Environment and Water: Canberra, Australia, 2022.
4. Hopkins, P. Pipelines: Past, Present, and Future. In Proceedings of the 5th Asian Pacific IIW International Congress, Sydney, Australia, 7–9 March 2007.
5. Victorian Government. *Gas and Pipeline Infrastructure Safety*; Performance Report, 2019–2020; Energy Safe Victoria: Melbourne, Australia, 2021.
6. Infrastructure Victoria. *Towards 2050: Gas Infrastructure in a Net Zero Emissions Economy*; Final report; Infrastructure Victoria: Melbourne, Australia, 2022.
7. Cech, M.; Davis, P.; Guijt, W.; Haskamp, A.; Barrio, I.H.; Valdenaire, D. *Performance of European Cross-Country Oil Pipelines—Statistical Summary of Reported Spillages in 2019 and Since 1971*; Concawe Special Task Force on-Oil Pipelines Performance Report (OP/STF-1); Concawe: Brussels, Belgium, 2021.
8. U.S. Department of Energy. *Natural Gas Infrastructure Modernization Programs at Local Distribution Companies: Key Issues and Considerations January 2017*; Office of Energy Policy and Systems Analysis, U.S. Department of Energy: Washington, DC, USA, 2017.
9. Fahimipirehgalin, M.; Trunzer, E.; Odenweller, M.; Vogel-Heuser, B. Automatic Visual Leakage Detection and Localization from Pipelines in Chemical Process Plants Using Machine Vision Techniques. *Engineering* **2021**, *7*, 758–776. [CrossRef]
10. Gresnigt, A.M.; Karamanos, S.A.; Andreadakis, K.P. Lateral Loading of Internally Pressurized Steel Pipes. *J. Press. Vessel. Technol.* **2007**, *129*, 630. [CrossRef]
11. Ramírez-Camacho, J.G.; Carbone, F.; Pastor, E.; Bubbico, R.; Casal, J. Assessing the consequences of pipeline accidents to support land-use planning. *Saf. Sci.* **2017**, *97*, 34–42. [CrossRef]
12. Biezma, M.V.; Andr'es, D.; Agudo, M.A.; Briz, E. Most fatal oil & gas pipeline accidents through history: A lessons learned approach. *Eng. Fail. Anal.* **2020**, *110*, 104446.
13. Bahaman, U.S.F.; Mustaffa, Z.; Seghier, M.E.A.B.; Badri, T.M. Evaluating the reliability and integrity of composite pipelines in the oil and gas sector: A scientometric and systematic analysis. *Ocean. Eng.* **2024**, *303*, 117773. [CrossRef]
14. Sirimanna, C.S.; Banerjee, S.; Karunasena, W.; Manalo, A.C.; McGarva, L. Analysis of retrofitted corroded steel pipes using internally bonded FRP composite repair systems. *Aust. J. Struct. Eng.* **2015**, *16*, 187–198. [CrossRef]
15. NEESR Group Cornell University. *Four-Point Bending Tests of Ductile Iron Pipe with Insituform IMain Liner 2011*; School of Civil and Environmental Engineering, Cornell University: Ithaca, NY, USA, 2011.
16. Kiriella, S.; Manalo, A.; Tien, C.M.T.; Ahmadi, H.; Wham, B.P.; Salah, A.; Tafsirojjaman, T.; Karunasena, W.; Dixon, P.; O'Rourke, T.D. Lateral deformation behaviour of structural internal replacement pipe repair systems. *Compos. Struct.* **2023**, *319*, 117144. [CrossRef]
17. Wham, B.P.; O'Rourke, T.D.; Senji, S.; Dixon, P.; Sickler, M.; Ihnotic, C.; Holt, D.; Strait, J.; Quandt, D. *Service Life Assessment of Internal Replacement Pipe: External Load Testing of ALTRA10*; Technical Report. Prepared for DOE/ARPA-E REPAIR; Center for Infrastructure, Energy, & Space Testing, University of Colorado Boulder & Geotechnical Lifelines Large-Scale Testing Facility; Cornell University: Ithaca, NY, USA, 2024.
18. Tafsirojjaman, T.; Manalo, A.; Tien, C.M.T.; Wham, B.P.; Salah, A.; Kiriella, S.; Karunasena, W.; Dixon, P. Analysis of failure modes in pipe-in-pipe repair systems for water and gas pipelines. *Eng. Fail. Anal.* **2022**, *140*, 106510. [CrossRef]
19. Tien, C.M.T.; Manalo, A.; Dixon, P.; Tafsirojjaman, T.; Karunasena, W.; Flood, W.W.; Ahmadi, H.; Kiriella, S.; Salah, A.; Wham, B.P. Effects of the legacy pipe ends on the behaviour of pipe-in-pipe repair systems under internal pressure. *Eng. Fail. Anal.* **2023**, *144*, 106957. [CrossRef]
20. Weber, R.L.; White, M.W.; Manning, K.V. *College Physics*; McGraw-Hill Book Company, Inc.: New York, NY, USA, 1952; 820p.
21. *ASTM A48/A48M-22*; Standard Specification for Gray Iron Castings. ASTM: West Conshohocken, PA, USA.
22. Ansys® Workbench. *Release 2021 R2, Help System*; ANSYS, Inc.: Canonsburg, PA, USA, 2021.
23. Bussieres, J. *Characterization of 4 Water Main CIPP Liner*; Centre de Developement des Composites du Quebec (CDCQ): Saint-Jérôme, QC, Canada, 2021.
24. *D5868-01*; Standard Test Method for Lap Shear Adhesion for Fiber Reinforced Plastic (FRP) Bonding. ASTM: West Conshohocken, PA, USA, 2014.
25. Mohammad, M.T.; Seyed, H.J.; Hossein, A.K. Lap shear strength and thermal stability of diglycidyl ether of bisphenol a/epoxy novolac adhesives with nanoreinforcing fillers. *J. Appl. Polym. Sci.* **2014**, *131*, 40017.

26. Kiriella, S.; Manalo, A.; Tien, C.M.T.; Ahmadi, H.; Dixon, P.G.; Karunasena, W.; Salah, A.; Wham, B.P. Bending fatigue behaviour of internal replacement pipe systems. *Compos. Struct.* **2024**, *331*, 117910. [CrossRef]
27. Stewart, H.E.; O'Rourke, T.D.; Wham, B.P.; Netravali, A.N.; Argyrou, C.; Zeng, X.; Bond, T.K. *Performance Testing of Field-Aged Cured-in-Place Liners (CIPL) for Cast Iron Piping 2015*; NYSEARCH/Northeast Gas Association: Boston, MA, USA, 2015; p. 114.
28. Kozman, D.P. Bonded or Unbonded Liners? How Longitudinal Bending Impacts Pipe Lining Design and Performance. In Proceedings of the American Society of Civil Engineers Pipelines 2020, San Antonio, TX, USA, 9–12 August 2020; pp. 263–270.
29. Ahmadi, H.; Manalo, A.; Dixon, P.G.; Salah, A.; Karunasena, W.; Tien, C.M.T.; Kiriella, S.; Wham, B.P.; O'Rourke, T.D. Temperature change-induced linear and nonlinear axial responses of internal replacement pipe (IRP) systems for pipeline rehabilitation incorporating the effects of soil friction. *Structures* **2024**, *62*, 106247. [CrossRef]